DOKUZ EYLÜL UNIVERSITY
GRADUATE SCHOOL OF NATURAL AND APPLIED SCIENCES

# MESH GENERATION AND ELECTRONIC STRUCTURE OF QUANTUM WIRES

by

Ümit DOĞAN

October, 2009
İZMİR

# MESH GENERATION
# AND
# ELECTRONIC STRUCTURE OF QUANTUM WIRES

**A Thesis Submitted to the**
**Graduate School of Natural and Applied Sciences of Dokuz Eylül University**
**In Partial Fulfillment of the Requirements for the Degree**
**of Doctor of Philosophy in**
**Physics**

**by**

**Ümit DOĞAN**

**October, 2009**
**İZMİR**

**Ph.D. THESIS EXAMINATION RESULT FORM**

We have read the thesis entitled **"MESH GENERATION AND ELECTRONIC STRUCTURE OF QUANTUM WIRES"** completed by **ÜMİT DOĞAN** under supervision of **PROF. DR. İSMAİL SÖKMEN** and we certify that in our opinion it is fully adequate, in scope and in quality, as a thesis for the degree of Doctor of Philosophy.

.....

Prof. Dr. İsmail SÖKMEN

Supervisor

.....

Doç. Dr. C. Cengiz ÇELİKOĞLU

Thesis Committee Member

.....

Prof. Dr. Doğan DEMİRHAN

Thesis Committee Member

.....

Yard. Doç. Dr. Görkem OYLUMLUOĞLU

Examining Committee Member

.....

Prof. Dr. Fevzi BÜYÜKKILIÇ

Examining Committee Member

Prof. Dr. Cahit HELVACI
Director
Graduate School of Natural and Applied Sciences

## ACKNOWLEDGEMENTS

It is a great pleasure for me to be at this point of my work when I have the opportunity to acknowledge and thank all the people who brought his contribution in a way or another during my PhD works.

First of all, I would like to express my deepest gratitude to my supervisor Prof. Dr. İsmail SÖKMEN for his excellent guidance, endless patience, continual encouragement and insightful suggestions throughout this work. His invaluable scientific contributions and enlightening on several physical concepts related to the theory and methods are irreplaceable for my further scientific carriers. I have greatly benefited from his thorough knowledge and expertise in semiconductor and computational physics. Professor SÖKMEN taught me not only his precious knowledge, but also his responsibility and strict attitude.

I am indebted to Assis. Prof. Dr. Kadir AKGÜNGÖR for much support, excellent motivation, fruitful discussions, valuable recommendations and contributions especially in preparation of the publications. This work would not been possible without his assistance in providing and administering excellent computer facilities.

This last paragraph I devote to people whom I am deeply emotionally connected with, my wonderful and loving family. Without their love and constant support nothing of this would be possible.

Ümit DOĞAN

## MESH GENERATION AND ELECTRONIC STRUCTURE OF QUANTUM WIRES

## ABSTRACT

In this thesis, single particle states in six different Quantum Wire cross-sections are studied by using Finite Element Method. In this case, energy values and charge localizations are given with arbitrary confinement potential profiles such as parabolic, linear and zero potentials. Mesh Generation which is necessary for the Finite Element Analysis, is presented as a brief overview.

This thesis also has detailed sections about the fundamental methods such as Finite Element Method, Area Coordinates, interpolation in d dimensions and the matrix elements of the generalized eigenvalue problem for the main problems.

In additional to single particle states with arbitrary potential profiles, exciton states in parabolic GaAs quantum dot is studied as a second problem. In this case, the energy spectrums of the exciton system versus confinement parameter and interaction parameter are showed in two energy scales. Because of the FEM is a powerful tool, the excited states are given with high accuracy in additional to ground state which can be obtained by using the traditional variational methods in the literature. Here again, charge localizations and the ground state energy data depending on quantum dot size has shown for different angular momentum quantum numbers.

The result of the calculations are in perfect agreement with the analytical solutions of the well-known and principle problems which are mentioned in the further sections in this study.

**Keywords:** quantum wire, mesh generation, finite element method, exciton

# AĞ GÖZÜ ÜRETİMİ VE KUANTUM TELLERİN ELEKTRONİK YAPISI

## ÖZ

Bu tezde, altı farklı kuantum tel çalışma uzayı içerisindeki tek parçacık için Sonlu Elemenlar Yöntemi ile yapılan sayısal hesaplar yapılmıştır. Bu anlamda tek parçacık durumları, enerji değerleri ve yük yerelleşmeleri hapsetme potansiyelinin olmadığı ve olduğu durumlarda (parabolik ve lineer hapsetmeler) verilmiştir. Sonlu elemanlar analizinden önce yapılması gerekli olan Ağ Gözü Üretimi konusu ise temel ve genel olarak ifade edilmiştir.

Tez, hesaplamalarda kullanılan kuramsal ve temel yöntemleri tanımlayan, anlatan ve açıklayan detaylı bölümlere sahiptir. Bu temel yöntemler ana hatlarıyla Sonlu Elemanlar Yöntemi, Alan Koordinatları, d boyut için interpolasyon ve genelleştirilmiş özdeğer eşitliği için matris temsillerinin bulunması olarak verilebilir.

Tek parçacık durumlarına ek olarak, parabolik GaAs kuantum noktasında ekziton durumları da ikinci bir problem olarak çalışılmıştır. Bu anlamda, ekziton enerji tayfı, hapsetme ve etkileşim parametrelerine bağlı olarak iki farklı enerji ölçeğinde çizilmiştir. Sonlu Elemanlar Yönteminin gücü sayesinde geleneksel varyasyonel yöntemlerle elde edilen taban durumunun yanısıra, uyarılmış üst enerji seviyeleri de yüksek duyarlılıkla hesaplanmıştır. Yine bu problem için de, yük yerelleşmeleri ve taban durum enerjisinin kuantum nokta büyüklüğüne göre grafiği verilmiştir.

Sayısal sonuçların elde edildiği yöntem ve programlar, tezin ilerleyen bölümlerinde sözü edilen, iyi bilinen ve analitik sonuçları belli olan temel problemler üzerinde denenmiş ve bu analitik sonuçlarla çok iyi uyuştuğu belirlenmiştir.

**Anahtar sözcükler:** kuantum tel, ağgözü üretimi, sonlu elemanlar yöntemi, ekziton

**CONTENTS**

# CHAPTER ONE
# INTRODUCTION

In the semiconductor physics, the virtual structures such as the movement of the electrons are trapped for example in one or two dimensions have very important role and have attracted attention in the literature for years (Proetto, 1992). The electrons are trapped in different directions in the two dimensional electron gas (2DEG) that in the hetero-structures made by fixing the semiconductors that has different energy band diagrams. The electron movement could be limited in one more direction by an electronic confinement in silicon metal oxide semiconductors or $GaAs$ / $Al_xGa_{1-x}As$ hetero-structures. The electron systems like this could be named as quantum wire (QW) (Proetto, 1992). The electronic structures of such systems can be obtained via the numerical solutions of the Schrödinger equation and the Poisson equation self consistently. Mesh Generation and *Finite Element Method (FEM)* (Pask et. al., 2001) could be used for the solution of these equations.

Two dimensional quantum confinement structures, called quantum wires (QW) as mentioned above, are innovate materials potentially applicable in optical devices such as laser diodes (Park et. al., 2004). The application of lower dimensional semiconductor structures as active regions of laser diodes promises improved device performance compared to the conventional quantum well (QWe) laser diodes. For one-dimensional structure, the density of states at the band edge is extremely high. This should lead to higher optical gain and thus very low threshold currents are predicted (Yariv, 1988; Arakawa, & Yariv, 1986).

In this work we proposed an efficient numerical method for calculating the electronic structure of low dimensional systems such as quantum dots and quantum wires including not only the ground state energy but also higher energy levels by using area coordinates and Finite Element Method. In this respect,

single charged particle problem under parabolic and linear confinement in six different quantum wire cross-sections are investigated. Also, an exciton system in a parabolic GaAs quantum dot problem is studied with high accuracy additional to single particle problem in QW. This problem has a high spherical symmetry. This allowed us to reduce the dimensionality of the problem from 3D to 1D. As mentioned above, all calculations are done with the numerical method called Finite element method. FEM is a very important tool of scientific and engineering analysis. Using area coordinates with FEM, especially in QW calculations, provides us a significant simplification to form the matrix elements and also to calculate the integrals in two dimensions.

Before the numerical calculations, the work spaces should be discretized in one, two or three dimensions. This process is generally called mesh generation (MG). MG has a wide range of applications and among them scientific calculations are dominant (Persson, 2005). A simple MG could be made by choosing nodes and a triangulating method with these nodes. In order to obtain the meshes initially the nodes are distributed randomly in the work space. Then, according the geometry of the problem and the boundary conditions the new node coordinates are determined in the discreet work space with the Force Equilibrium condition and Delaunay triangulation in order to increase the MG quality. Numerical solutions of the partial differential equations (PDE's) with the methods such as Finite Element Method (FEM) and Boundary Element Method, interpolation and imaging could be respected as the application areas of MG.

One of the main aims of this thesis is to understand the electronic structure of the quantum wires (QW), and also electron systems in quantum dots (QD). Increasing the quality of MG with FEM for Quantum Rods (Hu et. al., 2002) and Quantum Tetrapod (Giorgi et. al., 2005) systems could be counted for the future works of this thesis. Therefore, the electronic structures, charge localizations, electronic transitions in QW lattices, tunneling and optical properties could be

respected among the future works.

This work is organized as follows: In Chapter 2, a brief overview of Quantum Wires is given. Chapter 3 contains the theoretical and numerical basis and methods including MG as a brief overview, FEM, Area coordinates and higher order basis. The numerical results of the single particle states in different quantum wires and the exciton system in a parabolic quantum dot have been presented in Chapter 4. Chapter 5 summarizes our results as a conclusion.

# CHAPTER TWO
# QUANTUM WIRES

It has already been shown that the reduction in dimensionality produced by confining electrons (or holes) to a thin semiconductor layer leads to dramatic change in their behaviour. This principle can be developed by further reducing the dimensionality of the electron's environment from a two dimensional quantum well to a one dimensional quantum wire and eventually to a zero dimensional quantum dot (Harrison, 2002). It should be noted that there is more than one method about how quantum wires might be fabricated. Figure 2.1 gives a simple outline of how it can be done. A standard quantum well layer can be patterned with photolithography or perhaps electron-beam lithography, and etched to leave free standing strip of quantum well material; the latter may or may not be filled in with an overgrowth of the barrier material (in this case, such as $Ga_{1-x}Al_xAs$) Any charge carriers are still confined along the heterostructure growth $z-$axis, as they were in the quantum well, but in addition (provided the strip is narrow enough) they are now confined along an additional direction, either the $x-$ or the $y-$ axis, depending on the lithography.

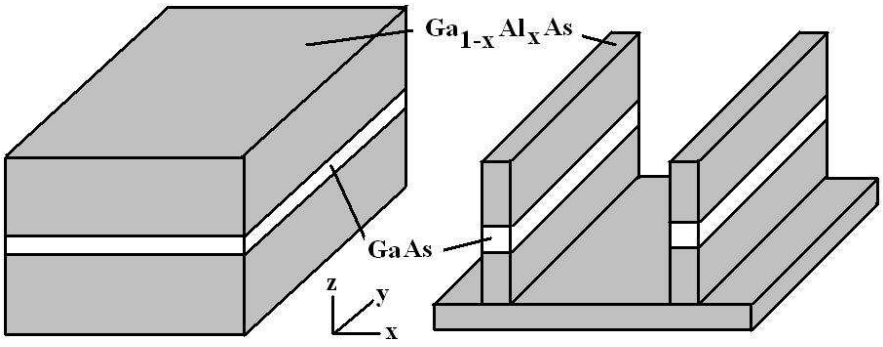


Figure 2.1 Fabrication of quantum wires

Figure 2.3 shows an expanded view of a single quantum wire, where clearly the electron (or hole) is free to move in only one direction, in this case along the

$y-$ axis. Within the effective-mass approximation the motion along the axis of the wire can still be described by a parabolic dispersion, i.e

$$E = \frac{\hbar^2 k^2}{2m^*} \tag{2.0.1}$$

just as in bulk and for in-plane motion within a quantum well (Harrison, 2002).

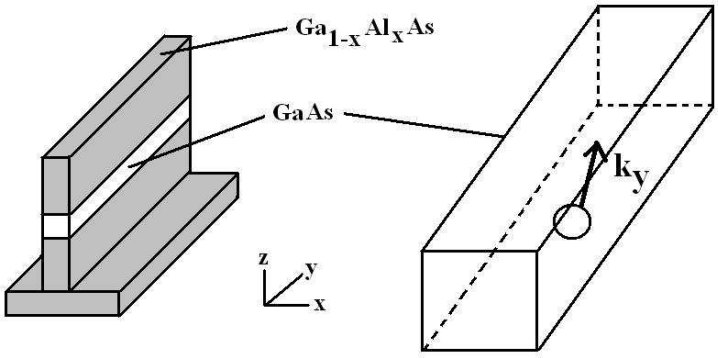


Figure 2.2 A single wire and an expanded view showing schematically the single degree of freedom in the electron momentum.

Another class of quantum wire can be formed by patterning the substrate before growth. This leads to the formation of so-called V-grooved wires (Kelly, 1995). The solution of these has been dealt with by Gangopadhyay, & Nag (1997).

After mentioning about the fabrication of the quantum wires, it is useful to give some information about the works of quantum wires in the literature. Two dimensional quantum confinement structures, called quantum wires (QW), are innovate materials potentially applicable in optical devices such as laser diodes (Park et. al., 2004). The application of lower dimensional semiconductor structures as active regions of laser diodes promises improved device performance compared to conventional quantum well (QWe) laser diodes. For one-dimensional structure, the density of states at the band edge is extremely high. This should lead to higher optical gain and thus very low threshold currents are predicted (Yariv, 1988; Arakawa, & Yariv, 1986).

Earlier methods to fabricate QWs involved removal of material from a QWe structure by etching (Lee et. al., 1988). Recent technological progress in the epitaxial growth led to various types of pseudomorphic QWs among which V-groove QWes have been intensively studied. Parallel to the effort concerning the fabrication and characterization of QWs, their theoretical modeling was also developed in order to enable the prediction of the physical properties of such structures and to enable a deeper understanding of experimental results. The calculations of the energy band diagram and the wave function of QWs are generally very complicated. In general, they cannot be done analytically, except for special circumstances such as isotropic cylindrical quantum wires with infinite potential barrier height (Sweeny et. al., 1988). Recently, several numerical techniques have been developed for the analysis of QW structures, which includes effective bond orbital method (EBOM) (Citrin, & Chang, 1989), tight binding method (TBM) (Yamauchi et. al., 1991), finite difference method (FDM) (Pryor, 1991), and finite-element method (FEM) (Searles, & von Nagy-Felsobuki, 1988; Kojima, & Mitsunaga, & Kyuma, 1989).

Although EBOM and TBM can describe the electronic band structure accurately, they require more than 18 basis functions at each atomic site, and as a result they require massive memory and processor time (Citrin, & Chang, 1989; Yamauchi et. al., 1991). However, FEM and FDM require only four and six basis function, respectively, depending on whether the spin-orbit split-off bands are neglected or not. The advantage of FEM as a numerical technique over FDM is that it can utilize a nonuniform mesh, hence the energy eigenstates and wave functions of arbitrarily shaped geometries with wide range of lateral dimensions can be analyzed accurately (Searles, & von Nagy-Felsobuki, 1988). Kojima, & Mitsunaga, & Kyuma (1989) calculated wave functions and energy levels of electrons in arbitrary shaped QW structures. Yi, & Dagli (1995) investigated valence band structures and optical properties of QW arrays on vicinal substrates using a four band kp analysis by FEM. Ogawa et. al. (1998) and

Ishigaki et. al. (2002) analyzed the valence band mixing effect, the strain effect, and the crystallographic orientation effect on the valence-subband structures of QWs using 4x4 Luttinger model by using the FEM. However, many fundamental properties such as effects of spin-orbit split-off bands on the valence band structure are not well known yet. In particular, there was not any comparison between two FDM and FEM methods to the best of our knowledge.

Park et. al. (2004) have investigated valence band structures of QWs by a calculation procedure based on a finite-element method. Here, the valence band structures are calculated by using the 6x6 Luttinger-Kohn Hamiltonian, which is a natural extension of the works of Ogawa et. al. (1998) and Ishigaki et. al. (2002). Park et. al. (2004) have also paid attention to effects of the spin-orbit split-off band in the valence band. That study considers an ordinary GaAs/AlGaAs QW system and numerical examples of triangular, square, and rectangular shape QWs are presented. In the case of square QW, results obtained by FEM are compared with those calculated by FDM.

In this thesis, the single particle states (excited states in addition to ground state) in 6 different QW cross-sections including parabolic and linear confinement profiles with Finite Element Method have been calculated with high accuracy. In a parabolic QD, exciton states, localizations and ground state energy data versus QD size are also presented.

# CHAPTER THREE
# THEORETICAL BASIS AND METHODS

## 3.1 Mesh Generation

This chapter is focused on the Mesh Generation that is necessary for the numerical calculation. Creating a mesh is the first step in a wide range of applications, including scientific computing and computer graphics. In the finite element approach to problems in greater than one dimension we are immediately faced with the complex issue of discretization of the physical domain. It is evident that for simple rectangular regions a straightforward breakup in the rectangles or triangles can be performed without any difficulty (Ram-Mohan, 2002).

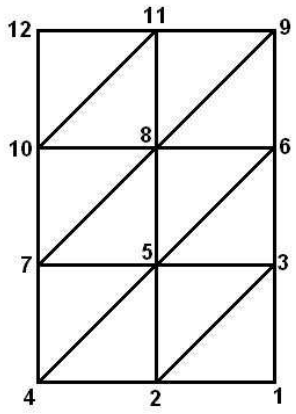


Figure 3.1 A regular grid of triangles for a rectangular region

As seen in Figure 3.1, the region is divided into rectangles which are then split up into a total of 12 triangular elements. Here it is employed the vector right hand rule to define the direction of the area vector of the each triangle to be out of the page. The three local node numbers are labeled as 1, 2 and 3 to correspond to this rule for each triangle. The global node numbers for a given triangle in the figure could have any value from 1 to the maximum number of the

nodes, and is determined by the mesh generator. While connecting the points in the desired manner to form the mesh, it is defined that the connectivity relation between the elements and the global node numbers. For example in Figure 3.1, the triangular corner element with global node index 12 has the three global nodes (12,10,11), in this order. it is required that two sets of data, one to specify the global coordinates $(x_i, y_i)$ for each node $i$, and the other to specify the global node numbers for the nodes in each element stated in the order with the positive area convention. This connectivity relation holds the key to placing the element matrices calculated in the Finite Element Method (FEM) in to a global matrix. The connectivity data should be generated and verified first, before any finite element calculation is performed.

When the nodes are connected together in a pattern and the connectivity is essentially independent of the location of the nodes, we have structured mesh, as in Figure 3.1. For physical regions with more complex boundaries it is required the creation what are called unstructured meshes. Any region with curved boundaries can be meshed using either quadrilateral or triangular elements. Typically, it is selected the location of nodal points on the boundaries and in the interior (Ram-Mohan, 2002). These points are connected to their neighbors in a way that varies from point to point leading to a lack of structure or pattern. Unstructured meshes have the advantage that they allows us to place of greater density of elements in regions where the solutions can be expected to vary rapidly. In this manner we can select a mesh such that it reflects the complexity in the solutions. In such unstructured meshes, setting up the connectivity relation between elements and the global numbering of their vertex nodes can be time consuming. As in structured meshes, the connectivity is again of primary importance. Automatic mesh generation algorithms have been devised that can use boundary nodes and generate a mesh in the interior with triangles that satisfy criteria suitable for finite element modeling in the following paragraphs.

An unstructured simplex mesh requires a choice of mesh points (vertex nodes) and a triangulation. The mesh should have small elements to resolve the fine details of geometry, but larger sizes where possible to reduce the total number of nodes. Furthermore, in numerical applications we need elements of high quality (for example triangles that are almost equilateral) to get accurate discretizations and well conditioned linear systems (Persson, 2005). One of the most popular meshing algorithms is the Delaunay refinement method (Ruppert, 1995; Shewchuk, 2002), which starts from an initial triangulation and refines until the element qualities are sufficiently high.

Many different mesh generation algorithms have been developed, and some of the most popular ones are described in the works by Bern, & Plassmann (1999) and Owen (1998). These methods usually work with explicit geometry representations, although many techniques have been proposed for triangulation of implicit surfaces (Bloomenthal, 1988; Figueiredo et. al., 1992; Desbrun et. al., 1996; Szeliski, & Tonnesen, 1992; Witkin, & Heckbert, 1994). Two more publications on mesh generations for level sets are Gloth, & Vilsmeier (2000) and Molino et. al. (2003).

In the numerical calculations that will be given in further sections of this thesis depend on the program codes by Persson (2005). These works are iterative techniques and based on simple mechanical analogy between a triangular mesh and a 2D truss structure, or equivalently a structure of springs. Any set of points in the x,y-plane can be triangulated by the Delaunay algorithm (Edelsbrunner, 2001). In the physical model, the edges of the triangles (the connections between pairs of points) correspond to bars, and points correspond to joints of the truss. Each bar has a force-displacement relationship $f(l, l_0)$ depending on its current length $l$ and its unextended length $l_0$. There are many alternatives for the force function $f(l, l_0)$ in each bar, and several choices have been investigated (Bossen, & Heckbert, 1996; Shimada, & Gossard, 1995). The function $k(l_0 - l)$ models

ordinary linear springs. Persson (2005)'s implementation uses this linear response for the repulsive forces but it allows no attractive forces:

$$f(l, l_0) = \begin{cases} k(l - l_0) & if \quad l < l_0 \\ 0 & if \quad l \geq 0 \end{cases} \tag{3.1.1}$$

Here $k$ is included to give correct units and set $k = 1$. The external forces on the structure come at the boundaries. At every boundary node, there is a reaction force acting normal to the boundary. The magnitude of this force is just large enough to keep the node from moving outside. The positions of the joints (these positions are the principal unknowns) are found by solving for a static force equilibrium in the structure (Persson, 2005).

## 3.2 Finite Element Method

In FEM that is a powerful numerical method for the solutions of the physical systems, the approximate solution of the system under consideration is searched in the finite function space and this finite function space can be described with a basis function set.

$$\{\phi_1, \phi_2, \phi_3, \cdots \phi_N\} \tag{3.2.1}$$

Here, $N$ is the dimension of the space. Any function member of the work space can be denoted as a linear combination of the basis functions. For example, the approximate solution that is searched for the exact solution in the discrete work space which has $z_N$ variables is:

$$U(z) = \sum_{j=1}^{N} c_j \phi_j(z) \tag{3.2.2}$$

Here, $c_j$'s are scalar constants. Rather frequently, the basis functions thats stretch the solution space are chosen as polynomial functions for finite polynomial space, because the polynomials have well known special features and can be described easily. In this case, the basis functions are the polynomials and the order of these polynomials is $N = n+1$ for the polynomial space thats order is $n$. For example, $\{1, z, z^2, ..., z^N\}$'s can be selected as the basis polynomials. But, there is no just one fundamental set for any linear vector space, therefore choosing the basis functions is flexible. We choose the *Lagrange Polynomials* (Pask et. al., 2001) as the basis functions for the polynomial space basis functions. Lagrange polynomials are described as $z_1, z_2, ..., z_N$ according to $N$ nodes in the work space $\Omega$. $(N-1)$.th degree polynomial is related to every $z_j$ and here, $j$ is the node index. The polynomials have this characteristic:

$$\phi_i(z_j) = \delta_{i,j} \tag{3.2.3}$$

If one consider there are $N$ nodes in the solution space, there will be $(N-1)$ part in the system which are $(\Omega_j)$ and everyone of these parts is between $\left(\frac{j-1}{N}, \frac{j}{N}\right)$ interval. Let us search the basis functions in the $z$ space and $\Omega = [-1, 1]$ interval. Consider the number of nodes is $N_0$ ($N_0 \geq 2$). Therefore the number of the basis functions is $N_0$ and their degree is like ($z^{N_0-1}$.). The polynomials which ensures $\phi_i(z_j) = \delta_{i,j}$ condition can be stated as following:

$$\phi_i(z) = \Lambda_i \prod_{i \neq j=1}^{N_0} (z - z_j) \tag{3.2.4}$$

$$\phi_i(z_k) = \Lambda_i \prod_{i \neq j=1}^{N_0} (z_k - z_j) \tag{3.2.5}$$

Here, $\Lambda_i$'s are the normalization constants.

$$\Lambda_i = \frac{1}{\prod_{i \neq j=1}^{N_0} (z_i - z_j)}$$

$$\phi_i(z_k) = \frac{\prod_{i \neq j=1}^{N_0} (z_k - z_j)}{\prod_{i \neq j=1}^{N_0} (z_i - z_j)} \tag{3.2.6}$$

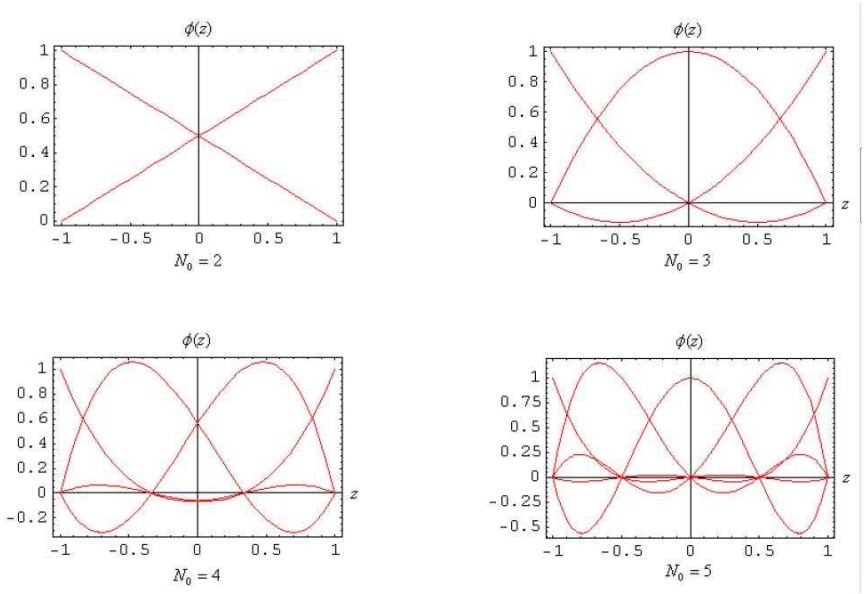


Figure 3.2 One dimensional basis functions in $z$ space for different number of nodes.

### *3.2.1 One Dimensional Linear Basis Functions*

Let us seek the basis functions for the work space $\Omega = (0, 1)$ as shown in Figure 3.2. The work space is divided three subspaces $(\Omega_1, \Omega_2, \Omega_3)$. The parent basis $\left\{\hat{\Omega}\right\}$ that is used in order to relate the local basis functions to every elements

are described over the parent element $\hat{\Omega} = (-1, 1)$. Therefore the parent basis become,

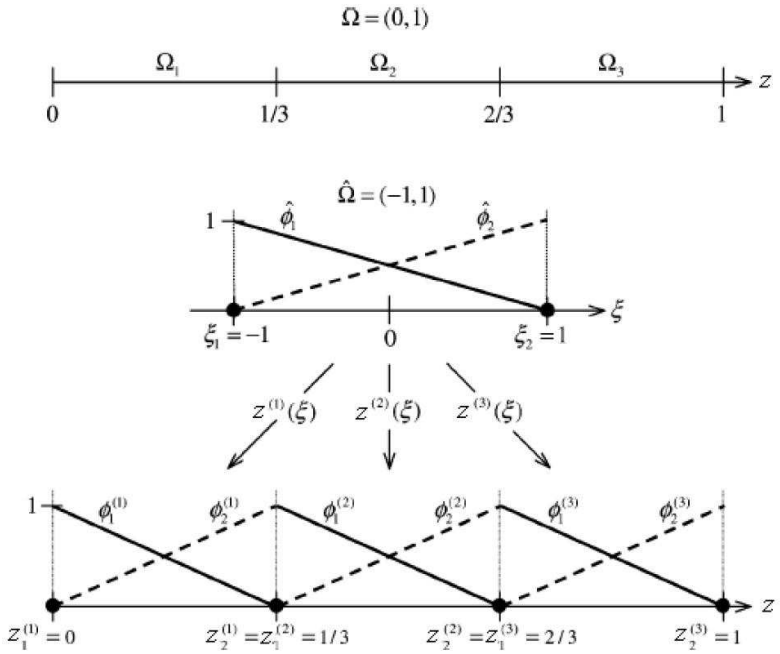


Figure 3.3 Three elements work space, linear basis functions and the global basis functions which are got after placing the basis into the work space between [-1,1] interval.

$$\begin{aligned} \hat{\phi}_1(\xi) = \tfrac{\xi-\xi_2}{\xi_1-\xi_2} = \tfrac{\xi-1}{-1-1} = -\tfrac{1}{2}(\xi-1) \quad &\rightarrow \quad \hat{\phi}_1(\xi) = -\tfrac{1}{2}(\xi-1) \\ \hat{\phi}_2(\xi) = \tfrac{\xi-\xi_1}{\xi_2-\xi_1} = \tfrac{\xi-(-1)}{-1-(-1)} = \tfrac{1}{2}(\xi+1) \quad &\rightarrow \quad \hat{\phi}_2(\xi) = \tfrac{1}{2}(\xi+1) \end{aligned} \tag{3.2.7}$$

The local basis functions related to every $\Omega_j$ elements are defined by a transformation $z^{(j)}(\xi)$ which is from the parent element $\hat{\Omega}$ to every $\Omega_j$ elements. One should get the relationship between $z$ and $\xi$ for this transformation.

$$z^{(j)}(\xi) = a^{(j)}\xi + b^{(j)} \tag{3.2.8}$$

$z^{(j)}(\xi)$'s are well known with the node indexes for $\xi = -1$ and $\xi = 1$ values.

$$\begin{aligned} z^{(j)}(\xi = -1) &= -a^{(j)} + b^{(j)} = \tfrac{j-1}{N} \\ z^{(j)}(\xi = 1) &= a^{(j)} + b^{(j)} = \tfrac{j}{N} \end{aligned} \tag{3.2.9}$$

Consequently,

$$a^{(j)} = \frac{1}{2N} \quad , \quad b^{(j)} = \frac{2j-1}{2N} \tag{3.2.10}$$

$$z^{(j)}(\xi) = \frac{1}{2N}\xi + \frac{2j-1}{2N} \tag{3.2.11}$$

And, by a reverse transformation,

$$\xi^{(j)}(\xi) = 2Nz + (1-2j) \tag{3.2.12}$$

Therefore, by taking $N = 3$ and $j = 1, 2, 3$ for every element;

$$\begin{aligned} z^{(1)}(\xi) &= \frac{1}{6}\xi + \frac{1}{6} \quad , \quad \xi^{(1)}(z) = 6z - 1 \\ z^{(2)}(\xi) &= \frac{1}{6}\xi + \frac{3}{6} \quad , \quad \xi^{(2)}(z) = 6z - 3 \\ z^{(3)}(\xi) &= \frac{1}{6}\xi + \frac{5}{6} \quad , \quad \xi^{(1)}(z) = 6z - 5 \end{aligned} \tag{3.2.13}$$

The expression for the local basis functions belonged to every elements is,

$$\phi_i^{(j)}(z) = \hat{\phi}_i \left[\xi^{(j)}(z)\right] \tag{3.2.14}$$

From this relation, we get

$$\phi_1^{(1)}(z) = 1 - 3z \quad , \quad \phi_2^{(1)}(z) = 3z$$

$$\phi_1^{(2)}(z) = 2 - 3z \quad , \quad \phi_2^{(2)}(z) = 3z - 1 \tag{3.2.15}$$

$$\phi_1^{(3)}(z) = 3 - 3z \quad , \quad \phi_2^{(3)}(z) = 3z - 2$$

Thus, piecewise global basis functions are got by combine the local functions at the collide nodes with each elements in the $z$ space.

$$\phi_1(z) = \left\{ \begin{array}{ccc} \phi_1^{(1)}(z) & , & z \in \Omega_1 \\ 0 & , & \text{other} \end{array} \right\}$$

$$\phi_2(z) = \left\{ \begin{array}{ccc} \phi_2^{(1)}(z) & , & z \in \Omega_1 \\ \phi_1^{(2)}(z) & , & z \in \Omega_2 \\ 0 & , & \text{other} \end{array} \right\}$$

$$\phi_3(z) = \left\{ \begin{array}{ccc} \phi_2^{(2)}(z) & , & z \in \Omega_2 \\ \phi_1^{(3)}(z) & , & z \in \Omega_3 \\ 0 & , & \text{other} \end{array} \right\} \tag{3.2.16}$$

$$\phi_4(z) = \left\{ \begin{array}{ccc} \phi_2^{(3)}(z) & , & z \in \Omega_3 \\ 0 & , & \text{other} \end{array} \right\}$$

### *3.2.2 Generalized Eigen Value Problem*

Finite Element Method (FEM) is an effective and powerful numerical method which can be used to solve the problems related to the physical systems (Hutton, 2004). In this subsection, it will be explained how to get generalized eigenvalue

equation with FEM. The Hamiltonian of one particle system in a confinement profile $V(\vec{r})$ in one dimension is;

$$H = -\frac{\hbar^2}{2m}\vec{\nabla}^2 + V(\vec{r}) \tag{3.2.17}$$

One can write down the Schrödinger equation with this Hamiltonian and get the dimensionless Hamiltonian with an energy and length scale. Choosing the dimensionless scale is arbitrary, thus they can be chosen Bohr radius and effective Hartree energy as dimensionless scales. In other words, the dimensionless Hamiltonian,

$$H = -\frac{1}{2}\vec{\nabla}^2 + V(\vec{r}) \tag{3.2.18}$$

Therefore the Schrödinger equation with this dimensionless Hamiltonian becomes,

$$H\Psi = \varepsilon\Psi \tag{3.2.19}$$

If the wave function $\Psi$ which describes the physical system is the exact wave function, then equation (3.2.19) is valid. How much the trial wave function close the exact wave function, this expression is valid so much. It could be made a proposal for the wave function which describes the physical system and wants to be get by the fundamental idea of variational principle.

$$\Psi \rightarrow \psi(\vec{r}) \rightarrow \text{trial wave function which wants to be got} \tag{3.2.20}$$

The main aim is achieving the wave function family which makes the energy of the system minimum by writing down the Schrödinger equation and solving this

equation via the minimization principle for the system with trial wave functions. The Schrödinger equation with this proposed wave function is,

$$H\psi = \varepsilon\psi \tag{3.2.21}$$

First of all, one should discreetizate the work space as the first step of the numerical calculations. Therefore the basis functions $\phi_n(\vec{r})$ of the relevant work space could be wrote down as a serial expansion.

$$\psi(\vec{r}) = \sum_{n=1}^{N_{top}} \psi_n \phi_n(\vec{r}) \tag{3.2.22}$$

Here $N_{top}$ is the total number of the nodes in the discreet work space. And, the matrix representation of equation (3.2.22) with all nodes in the related space is,

$$\psi(\vec{r}) = \{\phi(\vec{r})\}^T \cdot \{\psi\} \tag{3.2.23}$$

Here,

$$\{\phi(\vec{r})\}^T = (\phi_1(\vec{r}), \phi_2(\vec{r}), \phi_3(\vec{r}), \ldots \phi_N(\vec{r})) \tag{3.2.24}$$

$$\{\psi\}^T = (\psi_1, \psi_2, \psi_3, \ldots, \psi_N) \tag{3.2.25}$$

Thus, $N_{top}$ variational parameters which are desired to get can obtain with Galerkin's Method (Kwon, & Bang, 2000). Here the fundamental principle is writing down the Schrödinger equation with wanted wave function $\psi(\vec{r})$, multiplying the equation by hermitian conjugate of the wave function on the left hand side and taking integral of this expression in the work space, then finally, constituting the $G$ expression which will be minimalized by the

variational variables of the system. Namely,

$$G = \int_{\Omega} \psi(\vec{r})^{\dagger}(H - \varepsilon I)\psi(\vec{r})d\Omega \tag{3.2.26}$$

Here, $\psi(\vec{r})^{\dagger} = \{\psi\}^{\dagger} \cdot \{\phi(\vec{r})\}$ and $I$ is the unit matrix $(N \times N)$. Besides, if $\psi(\vec{r})$ is the exact solution of the system $G$ equals zero $(G = 0)$, if not $G \neq 0$. $(\psi, \psi^{\dagger})$ family which minimalize the $G$ expression also minimalize the energy of the system. If one write down the matrix representations of the wave function and hermitian conjugate of it,

$$G = \{\psi\}^{\dagger} \cdot \left[ \int_{\Omega} \{\phi(\vec{r})\}(H - \varepsilon I)\{\phi(\vec{r})\}^{T} d\Omega \right] \cdot \{\psi\} \tag{3.2.27}$$

is obtained. Symbolical variation of the $G$ is,

$$\frac{\partial G}{\partial \{\psi\}^{\dagger}} = 0 \tag{3.2.28}$$

Therefore,

$$\left[ \int_{\Omega} \{\phi\}(H - \varepsilon I)\{\phi\}^{T} \, d\Omega \right] \cdot \{\psi\} = 0 \tag{3.2.29}$$

Let us focus on the kinetic term in the Hamiltonian before writing down it clearly. This integral can be written as

$$-\int_{\Omega} \{\phi\} \cdot \vec{\nabla}^{2}\{\phi\}^{T} \cdot d\Omega = \int_{\Omega} \vec{\nabla}\{\phi\} \cdot \vec{\nabla}\{\phi\}^{T} \cdot d\Omega - \int_{\Omega} \vec{\nabla}(\{\phi\} \cdot \vec{\nabla}\{\phi\}^{T}) \cdot d\Omega \tag{3.2.30}$$

The second term of this last equation can be transformed to a surface integral

by Stokes Theorem that well known in the mathematical physics lectures. Thus the kinetic term becomes,

$$-\int_{\Omega} \{\phi\} \cdot \vec{\nabla}^2 \{\phi\}^T \cdot d\Omega = \int_{\Omega} \vec{\nabla}\{\phi\} \cdot \vec{\nabla}\{\phi\}^T \cdot d\Omega - \int_{\partial\Omega} \{\phi\}(\vec{\nabla}\{\phi\}^T) \cdot d\vec{\Gamma} \quad (3.2.31)$$

Considering the physical boundary conditions that tells us the wave function must decay on the surface of the solution space of the physical system, the surface term in equation (3.2.31) does not contribute to the kinetic term.

$$\{\phi\}_{\text{surface}} = 0 \quad (3.2.32)$$

Now writing down the Hamiltonian in equation (3.2.29) clearly,

$$\left[\int_{\Omega} d\Omega \left[\frac{1}{2}\vec{\nabla}\{\phi\} \cdot \vec{\nabla}\{\phi\}^T + \{\phi\}V(\vec{r})\{\phi\}^T\right]\right] \cdot \{\psi\} = \varepsilon \left[\int_{\Omega} d\Omega \{\phi\}\{\phi\}^T\right] \cdot \{\psi\} \quad (3.2.33)$$

is obtained. With a new representation,

$$\{\{K\}\} \cdot \{\psi\} = \varepsilon \{\{M\}\} \cdot \{\psi\} \quad (3.2.34)$$

Here, $\{\{K\}\}$ and $\{\{M\}\}$ are called Stifness Matrix and Mass Matris, respectively. Equation (3.2.34) is the generalized eigenvalue equation of the system. Obviously,

$$\{\{K\}\} = \int_{\Omega} d\Omega \left[\frac{1}{2}\vec{\nabla}\{\phi\} \cdot \vec{\nabla}\{\phi\}^T + \{\phi\}V(\vec{r})\{\phi\}^T\right] \quad (3.2.35)$$

$$\{\{M\}\} = \int_{\Omega} d\Omega \{\phi\}\{\phi\}^T \quad (3.2.36)$$

The integrals over the whole work space can be re-described as the summation of the integrals over the divided work space elements.

$$\int_{\Omega} d\Omega = \sum_{e=1}^{N_e} \int_{\Omega_e} d\Omega \tag{3.2.37}$$

Therefore,

$$\{\{k_e\}\} = \int_{\Omega_e} d\Omega \left[\frac{1}{2}\vec{\nabla}\{N\} \cdot \vec{\nabla}\{N\}^T + \{N\}V\{N\}^T\right] \qquad \Rightarrow \qquad \{\{K\}\} = \sum_{e=1}^{N_e} \{\{k_e\}\} \tag{3.2.38}$$

and

$$\{\{m_e\}\} = \int_{\Omega_e} d\Omega \{N\}\{N\}^T \tag{3.2.39}$$

can be written. Here $\{N\}$ is the global element basis function, $\{\phi\}$ is the whole space basis functions. As a consequence, the equations of the physical systems could be re-formed by using the method given above with quality MG, then it will be easy to solve them with generalized eigenvalue problem numerical routines.

## 3.3 Interpolation and Area Coordinates

Interpolation is the process of defining a function that takes on specified values at specified points (MolerMathWorks). In the other words, interpolation can be defined as calculating the unknown interval values (for example $x$ value in Figure 3.3 indicated blue color) from known values ($x(i)$ values shown in Figure 3.3 for $i = 1, 2, .., 5$) of a function in a discreet space generally. In this subsection, interpolation and area coordinates will be discussed.

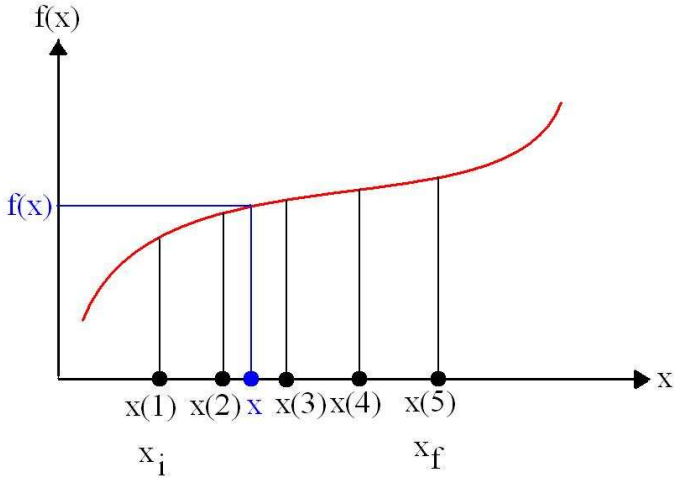


Figure 3.4 Illustration of interpolation of function $f(x)$ indicated red solid line.

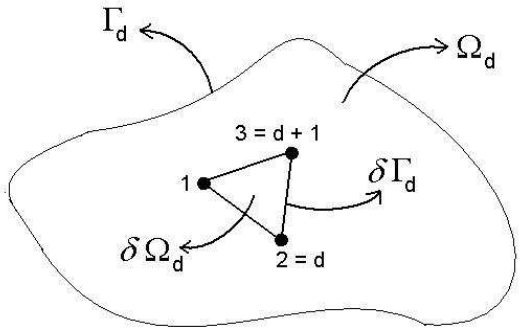


Figure 3.5 Illustration of a work space generally, the boundaries of it and a two dimensional global element

The arranged variables in $d$ dimensional space are,

$$x = (x_1, x_2, x_3, ...x_d) \tag{3.3.1}$$

A scalar field $F(x)$ in this space can be written as follows,

$$F(x) = a_0 + a_1x_1 + a_2x_2 + ... + a_dx_d \tag{3.3.2}$$

$i$ and $x(i)$ indicate the node number and the coordinates of the nodes, respectively. Thus,

$$F(x(i)) = a_0 + a_1x_1(i) + a_2x_2(i) + ... + a_dx_d(i) \tag{3.3.3}$$

$$F_i = F(x(i)) \tag{3.3.4}$$

Obviously for all nodes,

$$\begin{pmatrix} F_1 \\ F_2 \\ F_3 \\ . \\ . \\ F_{d+1} \end{pmatrix} = \begin{pmatrix} 1 & x_1(1) & x_2(1) & . & . & x_d(1) \\ 1 & x_1(2) & x_2(2) & . & . & x_d(2) \\ 1 & x_1(3) & x_2(3) & . & . & x_d(3) \\ . & . & . & . & . & . \\ . & . & . & . & . & . \\ 1 & x_1(d+1) & x_2(d+1) & . & . & x_d(d+1) \end{pmatrix} \begin{pmatrix} a_0 \\ a_1 \\ a_2 \\ . \\ . \\ a_d \end{pmatrix} \tag{3.3.5}$$

Here, one should mention about the notation that will be used in further parts.

For a matrix named $A$ (or a vector);

| | Matrix | Column Matrix | Row Matrix |
|---|---|---|---|
| For degenerate double bands | $\bar{\bar{A}}$ | $\bar{A}$ | $\bar{A}^T$ |
| For nodes | $\{\{A\}\}$ | $\{A\}$ | $\{A\}^T$ |

$$\{F\}^T = \begin{pmatrix} F_1 & F_2 & \cdots & F_{d+1} \end{pmatrix} \tag{3.3.6}$$

$$\{a\}^T = \begin{pmatrix} a_0 & a_1 & \cdots & a_d \end{pmatrix} \tag{3.3.7}$$

$$\{\{x\}\} = \begin{pmatrix} 1 & x_1(1) & x_2(1) & . & . & x_d(1) \\ 1 & x_1(2) & x_2(2) & . & . & x_d(2) \\ 1 & x_1(3) & x_2(3) & . & . & x_d(3) \\ . & . & . & . & . & . \\ . & . & . & . & . & . \\ 1 & x_1(d+1) & x_2(d+1) & . & . & x_d(d+1) \end{pmatrix} \tag{3.3.8}$$

In other words,

$$\{F\} = \{\{x\}\} \cdot \{a\} \tag{3.3.9}$$

$$\mathrm{Det}(\{\{x\}\}) = d! V_d \tag{3.3.10}$$

Here $V_d$ is the volume element in $d$ dimensional space.

$$a_0 = \frac{1}{\mathrm{Det}(\{\{x\}\})} \begin{vmatrix} F_1 & x_1(1) & x_2(1) & . & . & x_d(1) \\ F_2 & x_1(2) & x_2(2) & . & . & x_d(2) \\ F_3 & x_1(3) & x_2(3) & . & . & x_d(3) \\ . & . & . & . & . & . \\ . & . & . & . & . & . \\ F_{d+1} & x_1(d+1) & x_2(d+1) & . & . & x_d(d+1) \end{vmatrix} \tag{3.3.11}$$

Similarly, writing $\{F\}$ into $i$th column for $i$th $a$ coefficient ($a_i$),

$$a_i = \frac{1}{\mathrm{Det}(\{\{x\}\})} \begin{vmatrix} 1 & x_1(1) & . & F_1 & . & x_d(1) \\ 1 & x_1(2) & . & F_2 & . & x_d(2) \\ 1 & x_1(3) & . & F_3 & . & x_d(3) \\ . & . & . & . & . & . \\ . & . & . & . & . & . \\ 1 & x_1(d+1) & . & F_{d+1} & . & x_d(d+1) \end{vmatrix} \tag{3.3.12}$$

can be obtained. Again similarly for the coefficient $a_d$,

$$a_d = \frac{1}{\mathrm{Det}(\{\{x\}\})} \begin{vmatrix} 1 & x_1(1) & . & . & x_{d-1}(1) & F_1 \\ 1 & x_1(2) & . & . & x_{d-1}(2) & F_2 \\ 1 & x_1(3) & . & . & x_{d-1}(3) & F_3 \\ . & . & . & . & . & . \\ . & . & . & . & . & . \\ 1 & x_1(d+1) & . & . & x_{d-1}(d+1) & F_{d+1} \end{vmatrix} \tag{3.3.13}$$

Therefore, it can be written the general solution for the unknown $a_i$ coefficients as following equation.

$$a_i = \frac{1}{d!V_d}(-)^i \begin{vmatrix} F_1 & 1 & x_1(1) & . & x_{i-1}(1) & x_{i+1}(1) & . & x_d(1) \\ F_2 & 1 & x_1(2) & . & x_{i-1}(2) & x_{i+1}(2) & . & x_d(2) \\ F_3 & 1 & x_1(3) & . & x_{i-1}(3) & x_{i+1}(3) & . & x_d(3) \\ . & . & . & . & . & . & . & . \\ . & . & . & . & . & . & . & . \\ F_{d+1} & 1 & x_1(d+1) & . & x_{i-1}(d+1) & x_{i+1}(d+1) & . & x_d(d+1) \end{vmatrix} \tag{3.3.14}$$

It does not matter changing the rows and the columns of a matrix for the

determinant of the matrix. Thus, for the unknown $a_i$ coefficients,

$$a_i = \frac{1}{d!V_d}(-)^i \begin{vmatrix} F_1 & F_2 & . & . & F_{d+1} \\ 1 & 1 & . & . & 1 \\ x_1(1) & x_1(2) & . & . & x_1(d+1) \\ . & . & . & . & . \\ x_{i-1}(1) & x_{i-1}(2) & . & . & x_{i-1}(d+1) \\ x_{i+1}(1) & x_{i+1}(2) & . & . & x_{i+1}(d+1) \\ . & . & . & . & . \\ x_d(1) & x_d(2) & . & . & x_d(d+1) \end{vmatrix} \tag{3.3.15}$$

can be written.

$$F(x) = a_0 + a_1x_1 + a_2x_2 + \cdots + a_dx_d \tag{3.3.16}$$

If one puts these $a_i$ coefficients into the function $F(x)$, the function values $F_i$ can be find out.

$$F(x) = F_1L_1(x) + F_2L_2(x) + \cdots + F_{d+1}L_{d+1}(x) \tag{3.3.17}$$

$$i = 1, 2, \cdots, d, d+1; \quad x = (x_1, x_1, \cdots, x_d) \tag{3.3.18}$$

$$L_i(x) = \frac{1}{d!V_d}(-)^{(i-1)} \begin{vmatrix} 1 & x_1 & x_2 & . & . & x_d \\ 1 & x_1(1) & x_2(1) & . & . & x_d(1) \\ . & . & . & . & . & . \\ 1 & x_1(i-1) & x_2(i-1) & . & . & x_d(i-1) \\ 1 & x_1(i+1) & x_2(i+1) & . & . & x_d(i+1) \\ . & . & . & . & . & . \\ 1 & x_1(d+1) & x_2(d+1) & . & . & x_d(d+1) \end{vmatrix} \tag{3.3.19}$$

### *3.3.1 Area Coordinates ($L_i$)*

$d = 1$, $V_1 = (x(2) - x(1))$

$$L_1 = \frac{1}{V_1} \begin{vmatrix} 1 & x \\ 1 & x(2) \end{vmatrix} = \frac{(x(2) - x)}{(x(2) - x(1))} \tag{3.3.20}$$

$$L_2 = \frac{1}{V_1} \begin{vmatrix} 1 & x(1) \\ 1 & x \end{vmatrix} = \frac{(x - x(1))}{(x(2) - x(1))} \tag{3.3.21}$$

Node functions (basis);

$$N_1 = L_1 \tag{3.3.22}$$

$$N_2 = L_2$$

$$L_1 + L_2 = 1$$

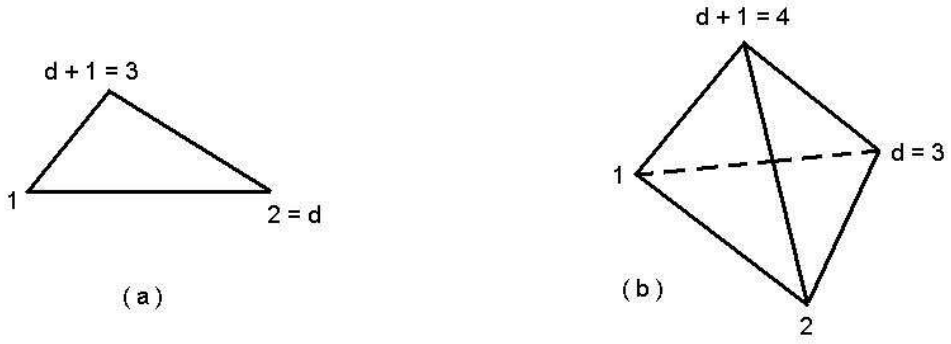


Figure 3.6 Choosing the global elements and naming the nodes (a) in two dimension (b) in three dimension

$d = 2$,

$$d!V_d = 2A$$

$$L_1 = \frac{1}{2A}\begin{vmatrix} 1 & x & y \\ 1 & x(2) & y(2) \\ 1 & x(3) & y(3) \end{vmatrix}$$

$$L_2 = \frac{1}{2A}\begin{vmatrix} 1 & x(1) & y(1) \\ 1 & x & y \\ 1 & x(3) & y(3) \end{vmatrix} \tag{3.3.23}$$

$$L_3 = \frac{1}{2A}\begin{vmatrix} 1 & x(1) & y(1) \\ 1 & x(2) & y(2) \\ 1 & x & y \end{vmatrix}$$

For the basis function with the area coordinates,

$$N_1(x,y) = L_1(x,y)$$

$$N_2(x,y) = L_2(x,y) \tag{3.3.24}$$

$$N_3(x,y) = L_3(x,y)$$

Similarly for three dimension, $d = 3$,

$$d!V_d = 6V$$

$$L_1 = \frac{1}{6V}\begin{vmatrix} 1 & x & y & z \\ 1 & x(2) & y(2) & z(2) \\ 1 & x(3) & y(3) & z(3) \\ 1 & x(4) & y(4) & z(4) \end{vmatrix}$$

$$L_2 = \frac{1}{6V}\begin{vmatrix} 1 & x(1) & y(1) & z(1) \\ 1 & x & y & z \\ 1 & x(3) & y(3) & z(3) \\ 1 & x(4) & y(4) & z(4) \end{vmatrix} \tag{3.3.25}$$

$$L_3 = \frac{1}{6V}\begin{vmatrix} 1 & x(1) & y(1) & z(1) \\ 1 & x(2) & y(2) & z(2) \\ 1 & x & y & z \\ 1 & x(4) & y(4) & z(4) \end{vmatrix}$$

$$L_4 = \frac{1}{6V}\begin{vmatrix} 1 & x(1) & y(1) & z(1) \\ 1 & x(2) & y(2) & z(2) \\ 1 & x(3) & y(3) & z(3) \\ 1 & x & y & z \end{vmatrix}$$

For the basis functions in three dimension there will be four $(3 + 1)$ basis functions.

$$\begin{aligned} N_1(x, y, z) &= L_1(x, y, z) \\ N_2(x, y, z) &= L_2(x, y, z) \\ N_3(x, y, z) &= L_3(x, y, z) \\ N_4(x, y, z) &= L_4(x, y, z) \end{aligned} \tag{3.3.26}$$

### *3.3.2 Jacobi Determinant*

We will show that, the Jacobi determinant in equation (3.3.10) is same with the volume element of the related work space in this sub section. The volume

element for $d$ dimensional space generally,

$$V_d = \int dx_1 \quad \int dx_2 \quad \int dx_3 \quad \cdots \int dx_d \tag{3.3.27}$$

$$dx_1 \quad dx_2 \quad \cdots \quad dx_d \quad = \quad J \quad dL_1 \quad dL_2 \quad \cdots \quad dL_d \tag{3.3.28}$$

Boundary condition for the area coordinates,

$$1 = L_1 + L_2 + \cdots + L_d + L_{d+1} \tag{3.3.29}$$

$$V_d \quad = \quad J \int_0^1 dL_1 \int_0^{1-L_1} dL_2 \int_0^{1-L_1-L_2} dL_3 \quad \cdots \int_0^{1-L_1-L_2-\cdots-L_{d-1}} dL_d \tag{3.3.30}$$

$$\int_0^{1-L_1-L_2-\cdots-L_{d-1}} dL_d \quad = \quad (1 - L_1 - L_2 - \cdots - L_{d-1})$$

$$\int_0^{1-L_1-L_2-\cdots-L_{d-2}} dL_{d-1}[(1 - L_1 - L_2 - \cdots - L_{d-2}) - L_{d-1}] \quad =$$

$$\frac{1}{2}(1 - L_1 - L_2 - \cdots - L_{d-2})^2$$

$$\int_0^{1-L_1-L_2-\cdots-L_{d-3}} dL_{d-2}\frac{1}{2}[(1 - L_1 - L_2 - \cdots - L_{d-3}) - L_{d-2}]^2$$

$$= \quad \frac{1}{2 \cdot 3}(1 - L_1 - L_2 - \cdots - L_{d-3})^3$$

$\cdots$

$$\int_0^1 dL_1 \cdot \frac{1}{2 \cdot 3 \cdot 4 \cdots (d-1)} \cdot (1 - L_1)^{d-1} = \frac{1}{2 \cdot 3 \cdot 4 \cdots d} = \frac{1}{d!} \tag{3.3.31}$$

$$V_d = J\frac{1}{d!} \quad \Rightarrow \quad J = d!V_d \tag{3.3.32}$$

One can see that equation (3.3.32) has the same meaning with equation (3.3.10).

### *3.3.3 The Integrals with Area Coordinates*

$$I = \int_0^1 dL_1 \quad \int_0^{1-L_1} dL_2 \quad \int_0^{1-L_1-L_2} dL_3 \quad \cdots \quad \int_0^{1-L_1-L_2-\cdots-L_{d-1}} dL_d \quad L_1^{n_1} L_2^{n_2} L_3^{n_3} \cdots L_d^{n_d} L_{d+1}^{n_{d+1}} \tag{3.3.33}$$

Boundary condition for the area coordinates again,

$$1 = L_1 + L_2 + \cdots + L_d + L_{d+1}$$

Beta Function;

$$B(p,q) = \int_0^1 du u^{p-1}(1-u)^{q-1} = \frac{\Gamma(p)\Gamma(q)}{\Gamma(p+q)} \tag{3.3.34}$$

$$\int_0^{1-L_1-L_2-\cdots-L_{d-1}} dL_d \quad L_d^{n_d} \quad (1-L_1-L_2-\cdots-L_{d-1}-L_d)^{n_{d+1}}$$

$$= (1-L_1-L_2\cdots-L_{d-1})^{n_d+1+n_{d+1}} \quad \left(\int_0^1 du \quad u^{n_d}(1-u)^{n_d+1}\right)$$

$$\left(\int_0^1 du \quad u^{n_d}(1-u)^{n_d+1}\right) = \frac{\Gamma(n_{d+1})\Gamma(n_{d+1}+1)}{\Gamma(n_d+n_{d+1}+1)} \tag{3.3.35}$$

Similarly,

$$\int_0^{1-L_1-L_2-\cdots-L_{d-2}} dL_{d-1} \quad L_{d-1}^{n_{d-1}} \quad (1-L_1-L_2-\cdots-L_{d-1})^{n_d+n_{d+1}+1}$$

$$= (1-L_1-L_2\cdots-L_{d-1})^{n_{d-1}+n_d+n_{d+1}+2} \quad \left(\int_0^1 du \quad u^{n_{d-1}}(1-u)^{n_d+n_{d+1}+1}\right)$$

$$\left(\int_0^1 du \quad u^{n_{d-1}}(1-u)^{n_d+n_{d+1}+1}\right) = \frac{\Gamma(n_{d-1}+1)\Gamma(n_d+n_{d+1}+2)}{\Gamma(n_{d-1}+n_d+n_{d+1}+3)} \tag{3.3.36}$$

.....

$$I = \frac{\Gamma(n_1+1)\Gamma(n_2+1)\cdots\Gamma(n_{d-1}+1)\Gamma(n_d+1)\Gamma(n_{d+1}+1)}{\Gamma(n_1+n_2+\cdots+n_{d-1}+n_d+n_{d+1}+(d+1))} \tag{3.3.37}$$

Therefore, the area coordinates for $i$th node and derivative of it can be written as follows.

$$L_i(x) = \frac{1}{d!V_d}(-)^{i-1} \cdot \begin{vmatrix} 1 & x_1 & x_2 & . & . & x_d \\ 1 & x_1(1) & x_2(1) & . & . & x_d(1) \\ . & . & . & . & . & . \\ 1 & x_1(i-1) & x_2(i-1) & . & . & x_d(i-1) \\ 1 & x_1(i+1) & x_2(i+1) & . & . & x_d(i+1) \\ . & . & . & . & . & . \\ 1 & x_1(d+1) & x_2(d+1) & . & . & x_d(d+1) \end{vmatrix} \tag{3.3.38}$$

$$\frac{\partial L_i(x)}{\partial x_j} = \frac{1}{d!V_d}(-)^{i-1}(-)^{j}. \tag{3.3.39}$$

$$\begin{vmatrix} 1 & x_1(1) & x_2(1) & . & x_{j-1}(1) & x_{j+1}(1) & . & x_d(1) \\ . & . & . & . & . & . & . & . \\ 1 & x_1(i-1) & x_2(i-1) & . & x_{j-1}(i-1) & x_{j+1}(i-1) & . & x_d(i-1) \\ 1 & x_1(i+1) & x_2(i+1) & . & x_{j-1}(i+1) & x_{j+1}(i+1) & . & x_d(i+1) \\ . & . & . & . & . & . & . & . \\ 1 & x_1(d+1) & x_2(d+1) & . & x_{j-1}(d+1) & x_{j+1}(d+1) & . & x_d(d+1) \end{vmatrix}$$

Here again,

$$i = 1, 2, 3, \cdots, d, d+1$$

$$j = 1, 2, 3, \cdots, d$$

$$J = d! V_d$$

$$V_d = \frac{1}{d!} \begin{vmatrix} 1 & x_1(1) & x_2(1) & . & . & x_d(1) \\ 1 & x_1(2) & x_2(2) & . & . & x_d(2) \\ . & . & . & . & . & . \\ 1 & x_1(d+1) & x_2(d+1) & . & . & x_d(d+1) \end{vmatrix} \tag{3.3.40}$$

### *3.3.4 Higher Order Basis Functions*

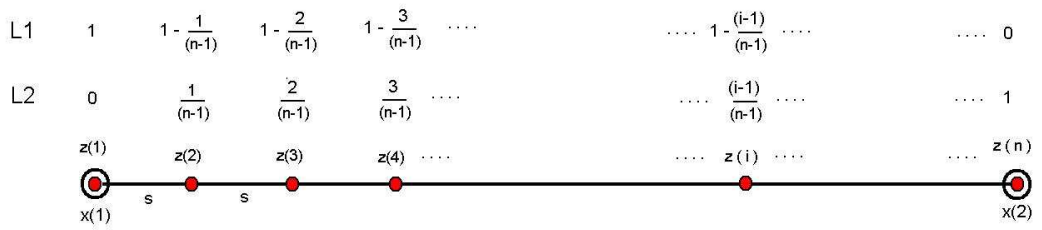


Figure 3.7 Illustrating of a global element in one dimension, global element nodes, coordinates and area coordinates for higher order basis functions.

$i = 1, 2, 3, \cdots, n, \quad n \rightarrow$ The node number in the global element

$$j = 2, 3, 4, \cdots, (n-1)$$

The coordinates of the nodes in the global element are,

$$z(j) = x(1) + (j-1)s, \qquad s = \frac{x(2) - x(1)}{(n-1)}$$

The node coordinates and the values of the area coordinates on the boundaries of the global element have shown in Figure 3.6. Thus,

$$J = 1! V_1 \begin{vmatrix} 1 & x(1) \\ 1 & x(2) \end{vmatrix} \tag{3.3.41}$$

$$J = V_1 = x(2) - x(1) = h$$

Therefore, for the area coordinates,

$$L_1 = \frac{1}{h} \begin{vmatrix} 1 & x \\ 1 & x(2) \end{vmatrix} \tag{3.3.42}$$

$$L_2 = -\frac{1}{h} \begin{vmatrix} 1 & x \\ 1 & x(1) \end{vmatrix}$$

$$L_1 = \left( \frac{x(2) - x}{x(2) - x(1)} \right) \tag{3.3.43}$$

$$L_2 = \left( \frac{x - x(1)}{x(2) - x(1)} \right)$$

For one dimension, the area coordinates $L_1$ and $L_2$ and the basis functions $N(L)$s related to area coordinates for the number of nodes in the global element

($N_{glo} = 2$),

$$N_1(x) = L_1(x) \tag{3.3.44}$$
$$N_2(x) = L_2(x)$$

$d = 1$, $N_{glo} = 3$; Here, it should be explained that basis functions in the global element have the form like the following equation. This relation makes simpler writing the basis functions with area coordinates.

$$(L_1 + L_2)^2 = L_1^2 + 2L_1L_2 + L_2^2$$

$$N_1(x) = 2L_1(L_1 - \frac{1}{2}) \tag{3.3.45}$$
$$N_2(x) = 4L_1L_2$$
$$N_3(x) = 2L_2(L_2 - \frac{1}{2})$$

$d = 1$, $N_{glo} = 4$;

$$(L_1 + L_2)^3 = L_1^3 + 3L_1^2L_2 + 3L_1L_2^2 + L_3^2$$

$$N_1(x) = L_1(L_1 - \frac{1}{3})(L_1 - \frac{2}{3})\frac{9}{2}$$
$$N_2(x) = L_1(L_1 - \frac{1}{3})L_2\frac{27}{2} \tag{3.3.46}$$
$$N_3(x) = L_1(L_2 - \frac{1}{3})L_2\frac{27}{2}$$
$$N_4(x) = L_2(L_2 - \frac{1}{3})(L_2 - \frac{2}{3})\frac{9}{2}$$

$d = 1$, $N_{glo} = 5$;

$$(L_1 + L_2)^4 = L_1^4 + 4L_1^3L_2 + 6L_1^2L_2^2 + 4L_1L_2^3 + L_4^2$$

$$\begin{aligned}
N_1(x) &= L_1(L_1 - \frac{1}{4})(L_1 - \frac{2}{4})(L_1 - \frac{3}{4})\frac{64}{6} \\
N_2(x) &= L_1(L_1 - \frac{1}{4})(L_1 - \frac{2}{4})L_2\frac{64 \cdot 4}{6} \\
N_3(x) &= L_1(L_1 - \frac{1}{4})(L_2 - \frac{1}{4})L_2\frac{64 \cdot 4}{4} \\
N_4(x) &= L_1(L_2 - \frac{2}{4})(L_2 - \frac{2}{4})L_2\frac{64 \cdot 4}{6} \\
N_5(x) &= (L_2 - \frac{3}{4})(L_2 - \frac{2}{4})(L_2 - \frac{1}{4})L_2\frac{64}{6}
\end{aligned} \tag{3.3.47}$$

Similarly; $d = 1$, $N_{glo} = 6$;

$$\begin{aligned}
N_1(x) &= L_1(L_1 - \frac{1}{5})(L_1 - \frac{2}{5})(L_1 - \frac{3}{5})(L_1 - \frac{4}{5})\frac{625}{24} \\
N_2(x) &= L_1(L_1 - \frac{1}{5})(L_1 - \frac{2}{5})(L_1 - \frac{3}{5})L_2\frac{3125}{24} \\
N_3(x) &= L_1(L_1 - \frac{1}{5})(L_1 - \frac{2}{5})(L_2 - \frac{1}{5})L_2\frac{3125}{12} \\
N_4(x) &= L_1(L_1 - \frac{1}{5})(L_2 - \frac{2}{5})(L_2 - \frac{1}{5})L_2\frac{3125}{12} \\
N_5(x) &= L_1(L_2 - \frac{3}{5})(L_2 - \frac{2}{5})(L_2 - \frac{1}{5})L_2\frac{3125}{24} \\
N_6(x) &= (L_2 - \frac{4}{5})(L_2 - \frac{3}{5})(L_2 - \frac{2}{5})(L_2 - \frac{1}{5})L_2\frac{625}{24}
\end{aligned} \tag{3.3.48}$$

$d = 1$, $N_{glo} = 7$;

$$N_1(x) = L_1(L_1 - \frac{1}{6})(L_1 - \frac{2}{6})(L_1 - \frac{3}{6})(L_1 - \frac{4}{6})(L_1 - \frac{5}{6})\frac{1296}{120}$$

$$N_2(x) = L_1(L_1 - \frac{1}{6})(L_1 - \frac{2}{6})(L_1 - \frac{3}{6})(L_1 - \frac{4}{6})L_2\frac{7776}{120}$$

$$N_3(x) = L_1(L_1 - \frac{1}{6})(L_1 - \frac{2}{6})(L_1 - \frac{3}{6})(L_2 - \frac{1}{6})L_2\frac{7776}{48}$$

$$N_4(x) = L_1(L_1 - \frac{1}{6})(L_1 - \frac{2}{6})(L_2 - \frac{2}{6})(L_2 - \frac{1}{6})L_2\frac{7776}{36} \tag{3.3.49}$$

$$N_5(x) = L_1(L_1 - \frac{1}{6})(L_2 - \frac{3}{6})(L_2 - \frac{2}{6})(L_2 - \frac{1}{6})L_2\frac{7776}{48}$$

$$N_6(x) = L_1(L_2 - \frac{4}{6})(L_2 - \frac{3}{6})(L_2 - \frac{2}{6})(L_2 - \frac{1}{6})L_2\frac{7776}{120}$$

$$N_7(x) = (L_2 - \frac{5}{6})(L_2 - \frac{4}{6})(L_2 - \frac{3}{6})(L_2 - \frac{2}{6})(L_2 - \frac{1}{6})L_2\frac{1296}{120}$$

$d = 1$, $N_{glo} = 8$;

$$N_1(x) = L_1(L_1 - \frac{1}{7})(L_1 - \frac{2}{7})(L_1 - \frac{3}{7})(L_1 - \frac{4}{7})(L_1 - \frac{5}{7})(L_1 - \frac{6}{7})\frac{117649}{720}$$

$$N_2(x) = L_1(L_1 - \frac{1}{7})(L_1 - \frac{2}{7})(L_1 - \frac{3}{7})(L_1 - \frac{4}{7})(L_1 - \frac{5}{7})L_2\frac{823543}{720}$$

$$N_3(x) = L_1(L_1 - \frac{1}{7})(L_1 - \frac{2}{7})(L_1 - \frac{3}{7})(L_1 - \frac{4}{7})(L_2 - \frac{1}{7})L_2\frac{823543}{240}$$

$$N_4(x) = L_1(L_1 - \frac{1}{7})(L_1 - \frac{2}{7})(L_1 - \frac{3}{7})(L_2 - \frac{2}{7})(L_2 - \frac{1}{7})L_2\frac{823543}{144}$$

$$N_5(x) = L_1(L_1 - \frac{1}{7})(L_1 - \frac{2}{7})(L_2 - \frac{3}{7})(L_2 - \frac{2}{7})(L_2 - \frac{1}{7})L_2\frac{823543}{144} \tag{3.3.50}$$

$$N_6(x) = L_1(L_1 - \frac{1}{7})(L_2 - \frac{4}{7})(L_2 - \frac{3}{7})(L_2 - \frac{2}{7})(L_2 - \frac{1}{7})L_2\frac{823543}{240}$$

$$N_7(x) = L_1(L_2 - \frac{5}{7})(L_2 - \frac{4}{7})(L_2 - \frac{3}{7})(L_2 - \frac{2}{7})(L_2 - \frac{1}{7})L_2\frac{823543}{720}$$

$$N_8(x) = (L_2 - \frac{6}{7})(L_2 - \frac{5}{7})(L_2 - \frac{4}{7})(L_2 - \frac{3}{7})(L_2 - \frac{2}{7})(L_2 - \frac{1}{7})L_2\frac{117649}{720}$$

### *3.3.5 2D Basis*

$d = 2$, $N_{glo} = 3$; **(T3)**

$$L_1(x,y) = \frac{1}{2!A}\begin{vmatrix} 1 & x & y \\ 1 & x_2 & y_2 \\ 1 & x_3 & y_3 \end{vmatrix} \tag{3.3.51}$$

$$L_2(x,y) = \frac{1}{2!A}\begin{vmatrix} 1 & x_1 & y_1 \\ 1 & x & y \\ 1 & x_3 & y_3 \end{vmatrix} \tag{3.3.52}$$

$$L_3(x,y) = \frac{1}{2!A}\begin{vmatrix} 1 & x_1 & y_1 \\ 1 & x_2 & y_2 \\ 1 & x & y \end{vmatrix} \tag{3.3.53}$$

Now, we can write the higher order basis functions such as linear, quadratic, cubic, quartic basis with equations (3.3.51), (3.3.52) ve (3.3.53) in two dimensions.

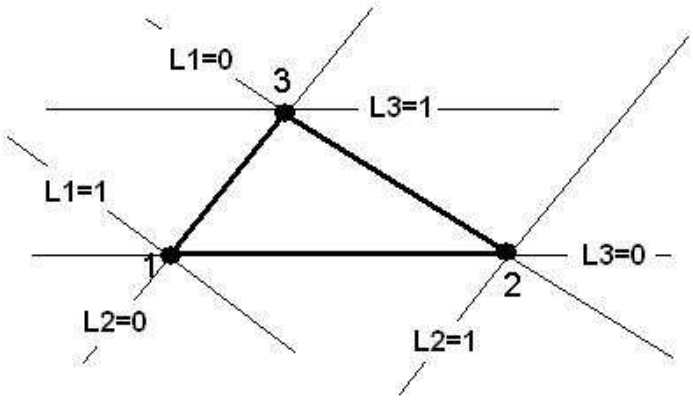


Figure 3.8 Illustrating of T3 Global element, linear basis

$$N_1(x,y) = L_1(x,y) \tag{3.3.54}$$

$$N_2(x,y) = L_2(x,y)$$

$$N_3(x,y) = L_3(x,y)$$

$d = 2$, **(T6)**

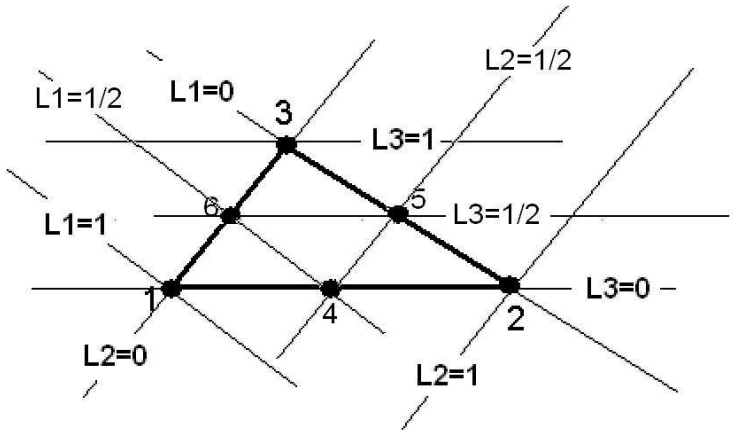


Figure 3.9 Illustrating of T6 Global element, quadratic basis

$$(L_1 + L_2 + L_3)^2 = L_1^2 + L_2^2 + L_3^2 + 2L_1L_2 + 2L_1L_3 + 2L_2L_3$$

$$N_1 = L_1(L_1 - \frac{1}{2}) \cdot 2$$

$$N_2 = L_2(L_2 - \frac{1}{2}) \cdot 2$$

$$N_3 = L_3(L_3 - \frac{1}{2}) \cdot 2 \tag{3.3.55}$$

$$N_4 = L_1L_2 \cdot 4$$

$$N_5 = L_2L_3 \cdot 4$$

$$N_6 = L_1L_3 \cdot 4$$

$d = 2$, **(T10)**

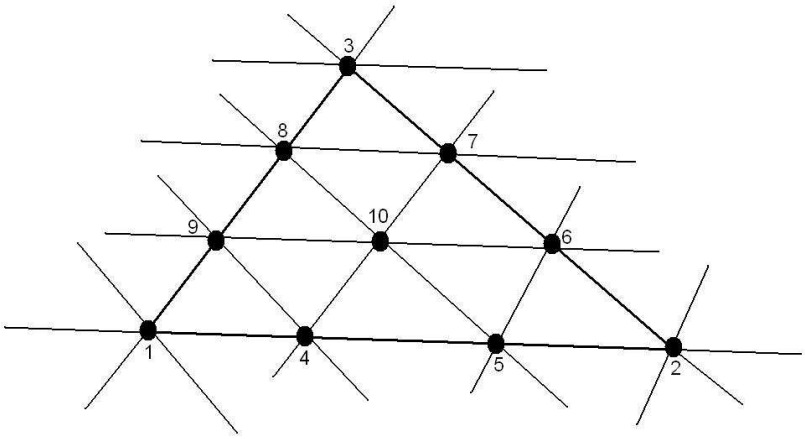


Figure 3.10 Illustrating of T10 Global element, cubic basis

$$(L_1 + L_2 + L_3)^3 = L_1^3 + L_2^3 + L_3^3 + 3L_1^2L_2 +$$

$$3L_1L_2^2 + 3L_1^2L_3 + 3L_1L_3^2 + 3L_2^2L_3 + 3L_2L_3^2 + 6L_1L_2L_3$$

$$\begin{aligned}
N_1 &= L_1(L_1 - \frac{1}{3})(L_1 - \frac{2}{3}) \cdot \frac{9}{2} \\
N_2 &= L_2(L_2 - \frac{1}{3})(L_2 - \frac{2}{3}) \cdot \frac{9}{2} \\
N_3 &= L_3(L_3 - \frac{1}{3})(L_3 - \frac{2}{3}) \cdot \frac{9}{2} \\
N_4 &= L_2(L_2 - \frac{1}{3})L_1 \cdot \frac{27}{2} \\
N_5 &= L_2(L_2 - \frac{1}{3})L_1 \cdot \frac{27}{2} \\
N_6 &= L_3(L_2 - \frac{1}{3})L_2 \cdot \frac{27}{2} \\
N_7 &= L_3(L_3 - \frac{1}{3})L_2 \cdot \frac{27}{2} \\
N_8 &= L_3(L_3 - \frac{1}{3})L_1 \cdot \frac{27}{2} \\
N_9 &= L_3(L_1 - \frac{1}{3})L_1 \cdot \frac{27}{2}
\end{aligned} \tag{3.3.56}$$

$$N_{10} = L_3 L_2 L_1 \cdot 27$$

$d = 2$, **(T15)**

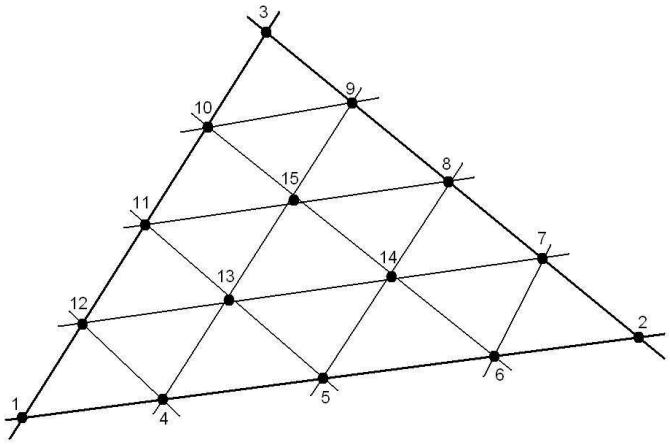


Figure 3.11 Illustrating of T15 Global element, quartic basis

$$\begin{aligned}
N_1 &= (L_1 - \frac{3}{4})(L_1 - \frac{2}{4})(L_1 - \frac{1}{4})L_1 \cdot \frac{64}{6} \\
N_2 &= (L_2 - \frac{3}{4})(L_2 - \frac{2}{4})(L_2 - \frac{1}{4})L_2 \cdot \frac{64}{6} \\
N_3 &= (L_3 - \frac{3}{4})(L_3 - \frac{2}{4})(L_3 - \frac{1}{4})L_3 \cdot \frac{64}{6} \\
N_4 &= (L_1 - \frac{2}{4})(L_1 - \frac{1}{4})L_1 L_2 \cdot \frac{128}{3} \\
N_5 &= (L_1 - \frac{1}{4})(L_2 - \frac{1}{4})L_1 L_2 \cdot 64 \\
N_6 &= (L_2 - \frac{1}{4})(L_2 - \frac{2}{4})L_1 L_2 \cdot \frac{128}{3} \\
N_7 &= (L_2 - \frac{1}{4})(L_2 - \frac{2}{4})L_3 L_2 \cdot \frac{128}{3} \\
N_8 &= (L_2 - \frac{1}{4})(L_3 - \frac{1}{4})L_3 L_2 \cdot 64 \\
N_9 &= (L_3 - \frac{1}{4})(L_3 - \frac{2}{4})L_3 L_2 \cdot \frac{128}{3}
\end{aligned} \tag{3.3.57}$$

$$N_{10} = (L_3 - \frac{1}{4})(L_3 - \frac{2}{4})L_3L_1 \cdot \frac{128}{3}$$

$$N_{11} = (L_3 - \frac{1}{4})(L_1 - \frac{1}{4})L_3L_1 \cdot 64$$

$$N_{12} = (L_1 - \frac{1}{4})(L_1 - \frac{2}{4})L_3L_1 \cdot \frac{128}{3}$$

$$N_{13} = (L_1 - \frac{1}{4})L_3L_2L_1 \cdot 128$$

$$N_{14} = (L_2 - \frac{1}{4})L_3L_2L_1 \cdot 128$$

$$N_{15} = (L_3 - \frac{1}{4})L_3L_2L_1 \cdot 128$$

$d = 2$, **(T21)**

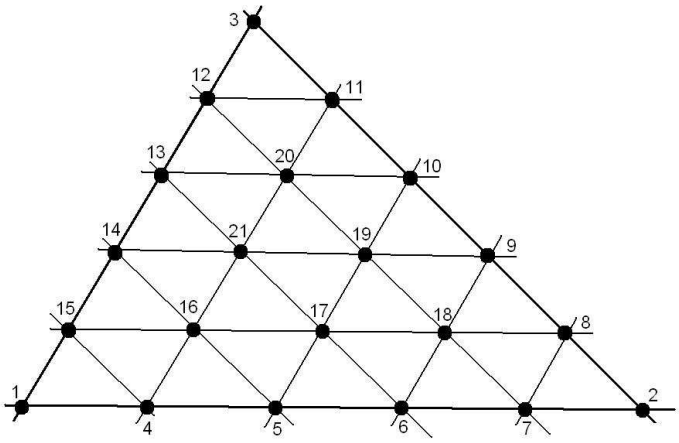


Figure 3.12 Illustrating of T21 Global element

$$N_1 = (L_1 - \frac{4}{5})(L_1 - \frac{3}{5})(L_1 - \frac{2}{5})(L_1 - \frac{1}{5})L_1 \cdot \frac{625}{24}$$

$$N_2 = (L_2 - \frac{4}{5})(L_2 - \frac{3}{5})(L_2 - \frac{2}{5})(L_2 - \frac{1}{5})L_2 \cdot \frac{625}{24}$$

$$N_3 = (L_3 - \frac{4}{5})(L_3 - \frac{3}{5})(L_3 - \frac{2}{5})(L_3 - \frac{1}{5})L_3 \cdot \frac{625}{24}$$

$$N_4 = (L_1 - \frac{3}{5})(L_1 - \frac{2}{5})(L_1 - \frac{1}{5})L_1L_2 \cdot \frac{3125}{24}$$

$$
\begin{aligned}
N_5 &= (L_1 - \frac{2}{5})(L_1 - \frac{1}{5})L_1L_2(L_2 - \frac{1}{5}) \cdot \frac{3125}{12} \\
N_6 &= (L_1 - \frac{1}{5})L_1L_2(L_2 - \frac{1}{5})(L_2 - \frac{2}{5}) \cdot \frac{3125}{12} \\
N_7 &= L_1L_2(L_2 - \frac{1}{5})(L_2 - \frac{2}{5})(L_2 - \frac{3}{5}) \cdot \frac{3125}{24} \\
N_8 &= (L_2 - \frac{3}{5})(L_2 - \frac{2}{5})(L_2 - \frac{1}{5})L_2L_3 \cdot \frac{3125}{24} \\
N_9 &= (L_2 - \frac{2}{5})(L_2 - \frac{1}{5})L_2L_3(L_3 - \frac{1}{5}) \cdot \frac{3125}{12} \\
N_{10} &= (L_2 - \frac{1}{5})L_2L_3(L_3 - \frac{1}{5})(L_3 - \frac{2}{5}) \cdot \frac{3125}{12} \\
N_{11} &= (L_3 - \frac{3}{5})(L_3 - \frac{2}{5})(L_3 - \frac{1}{5})L_3L_2 \cdot \frac{3125}{24} \\
N_{12} &= (L_3 - \frac{3}{5})(L_3 - \frac{2}{5})(L_3 - \frac{1}{5})L_3L_1 \cdot \frac{3125}{24} \\
N_{13} &= (L_1 - \frac{1}{5})L_1L_3(L_3 - \frac{1}{5})(L_3 - \frac{2}{5}) \cdot \frac{3125}{12} \\
N_{14} &= (L_1 - \frac{1}{5})L_1L_3(L_1 - \frac{2}{5})(L_3 - \frac{1}{5}) \cdot \frac{3125}{12} \\
N_{15} &= (L_1 - \frac{1}{5})(L_1 - \frac{2}{5})(L_1 - \frac{3}{5})L_1L_3 \cdot \frac{3125}{24} \\
N_{16} &= (L_1 - \frac{1}{5})(L_1 - \frac{2}{5})L_1L_2L_3 \cdot \frac{3125}{6} \\
N_{17} &= (L_1 - \frac{1}{5})(L_2 - \frac{1}{5})L_1L_2L_3 \cdot \frac{3125}{4} \\
N_{18} &= (L_2 - \frac{1}{5})(L_2 - \frac{2}{5})L_1L_2L_3 \cdot \frac{3125}{6} \\
N_{19} &= (L_2 - \frac{1}{5})(L_3 - \frac{1}{5})L_1L_2L_3 \cdot \frac{3125}{4} \\
N_{20} &= (L_3 - \frac{1}{5})(L_3 - \frac{2}{5})L_1L_2L_3 \cdot \frac{3125}{6} \\
N_{21} &= (L_1 - \frac{1}{5})(L_3 - \frac{1}{5})L_1L_2L_3 \cdot \frac{3125}{4}
\end{aligned}
\tag{3.3.58}
$$

### *3.3.6 3D Basis*

$$L_1(x,y,z) = \frac{1}{3!V}\begin{vmatrix} 1 & x & y & z \\ 1 & x_2 & y_2 & z_2 \\ 1 & x_3 & y_3 & z_3 \\ 1 & x_4 & y_4 & z_4 \end{vmatrix} \tag{3.3.59}$$

$$L_2(x,y,z) = \frac{1}{3!V}\begin{vmatrix} 1 & x_1 & y_1 & z_1 \\ 1 & x & y & z \\ 1 & x_3 & y_3 & z_3 \\ 1 & x_4 & y_4 & z_4 \end{vmatrix} \tag{3.3.60}$$

$$L_3(x,y,z) = \frac{1}{3!V}\begin{vmatrix} 1 & x_1 & y_1 & z_1 \\ 1 & x_2 & y_2 & z_2 \\ 1 & x & y & z \\ 1 & x_4 & y_4 & z_4 \end{vmatrix} \tag{3.3.61}$$

$$L_4(x,y,z) = \frac{1}{3!V}\begin{vmatrix} 1 & x_1 & y_1 & z_1 \\ 1 & x_2 & y_2 & z_2 \\ 1 & x_3 & y_3 & z_3 \\ 1 & x & y & z \end{vmatrix} \tag{3.3.62}$$

The global element basis functions also called the shape functions. Similarly to two dimensions, we can write the higher order basis functions such as linear, quadratic, cubic, quartic basis with equations (3.3.59),(3.3.60),(3.3.61) ve (3.3.62) in three dimensions.

$d = 3$, **(Linear Basis)**

$$N_1(x,y,z) = L_1(x,y,z)$$

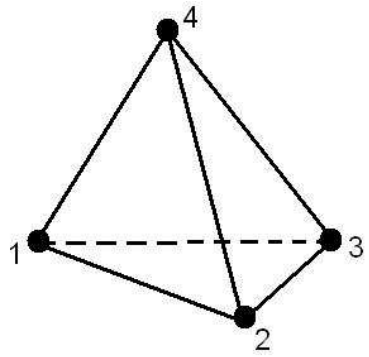


Figure 3.13 Illustrating of 3D Global element which has 4 nodes

$$N_2(x,y,z) = L_2(x,y,z) \tag{3.3.63}$$

$$N_3(x,y,z) = L_3(x,y,z)$$

$$N_4(x,y,z) = L_4(x,y,z)$$

$d = 3$, **(Quadratic Basis)**

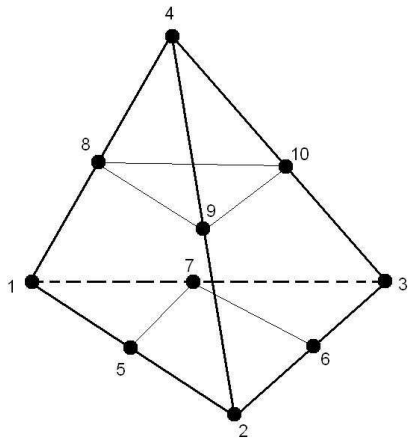


Figure 3.14 Illustrating of 3D Global element which has 10 nodes

$$N_1 = L_1(L_1 - \frac{1}{2}) \cdot 2$$

$$N_2 = L_2(L_2 - \frac{1}{2}) \cdot 2$$

$$N_3 = L_3(L_3 - \frac{1}{2}) \cdot 2$$

$$N_4 = L_4(L_4 - \frac{1}{2}) \cdot 2$$

$$N_5 = L_2L_1 \cdot 4 \tag{3.3.64}$$

$$N_6 = L_2L_3 \cdot 4$$

$$N_7 = L_3L_1 \cdot 4$$

$$N_8 = L_1L_4 \cdot 4$$

$$N_9 = L_2L_4 \cdot 4$$

$$N_{10} = L_4L_3 \cdot 4$$

$d = 3$, **(Cubic Basis)**

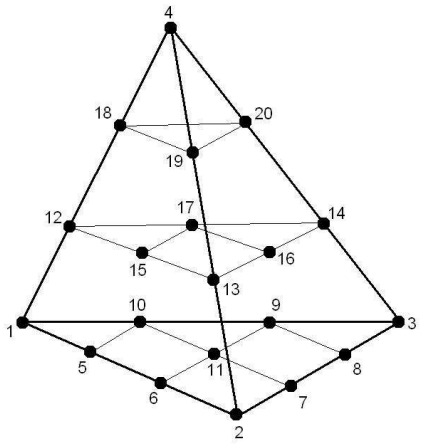


Figure 3.15 Illustrating of 3D Global element which has 20 nodes

$$N_1 = (L_1 - \frac{2}{3})(L_1 - \frac{1}{3})L_1 \cdot \frac{9}{2}$$

$$
\begin{aligned}
N_2 &= (L_2 - \frac{2}{3})(L_2 - \frac{1}{3})L_2 \cdot \frac{9}{2} \\
N_3 &= (L_3 - \frac{2}{3})(L_3 - \frac{1}{3})L_3 \cdot \frac{9}{2} \\
N_4 &= (L_4 - \frac{2}{3})(L_4 - \frac{1}{3})L_4 \cdot \frac{9}{2} \\
N_5 &= (L_1 - \frac{1}{3})L_1L_2 \cdot \frac{27}{2} \\
N_6 &= (L_2 - \frac{1}{3})L_1L_2 \cdot \frac{27}{2} \\
N_7 &= (L_2 - \frac{1}{3})L_3L_2 \cdot \frac{27}{2} \\
N_8 &= (L_3 - \frac{1}{3})L_3L_2 \cdot \frac{27}{2} \\
N_9 &= (L_3 - \frac{1}{3})L_3L_1 \cdot \frac{27}{2} \\
N_{10} &= (L_1 - \frac{1}{3})L_3L_1 \cdot \frac{27}{2} \\
N_{11} &= L_3L_2L_1 \cdot 27 \\
N_{12} &= (L_1 - \frac{1}{3})L_4L_1 \cdot \frac{27}{2} \\
N_{13} &= (L_2 - \frac{1}{3})L_4L_2 \cdot \frac{27}{2} \\
N_{14} &= (L_3 - \frac{1}{3})L_4L_3 \cdot \frac{27}{2} \\
N_{15} &= L_4L_2L_1 \cdot 27 \\
N_{16} &= L_4L_2L_3 \cdot 27 \\
N_{17} &= L_4L_3L_1 \cdot 27 \\
N_{18} &= (L_4 - \frac{1}{3})L_4L_1 \cdot \frac{27}{2} \\
N_{19} &= (L_4 - \frac{1}{3})L_4L_2 \cdot \frac{27}{2} \\
N_{20} &= (L_4 - \frac{1}{3})L_4L_3 \cdot \frac{27}{2}
\end{aligned}
\tag{3.3.65}
$$

### *3.3.7 The Interpolating Polynomial*

We all know that two points determine a straight line. More precisely, any two points in the plane, $(x_1, y_1)$ and $(x_2, y_2)$, with $x_1 \neq x_2$ determine a unique first degree polynomial in x whose graph passes through the two points. There are many different formulas for the polynomial, but they all lead to the same straight line graph.

This generalizes to more than two points. Given $n$ points in the plane, $(x_k, y_k)$; $k = 1, \cdots, n$, with distinct $x_k$'s, there is a unique polynomial in $x$ of degree less than $n$ whose graph passes through the points. It is easiest to remember that $n$, the number of data points, is also the number of coefficients, although some of the leading coefficients might be zero, so the degree might actually be less than $n - 1$. Again, there are many different formulas for the polynomial, but they all define the same function. This polynomial is called the interpolating polynomial because it exactly reproduces the given data (Moler, 2004):

$$P(x_k) = y_k, \quad k = 1, 2, ..., n. \tag{3.3.66}$$

The most compact representation of the interpolating polynomial is the Lagrange form

$$P(x) = \sum_k \left( \prod_{j \neq k} \frac{x - x_j}{x_k - x_j} \right) \tag{3.3.67}$$

There are $n$ terms in the sum and $n-1$ terms in each product, so this expression defines a polynomial of degree at most $n - 1$. If $P(x)$ is evaluated at $x = x_k$, all the products except the $k$th are zero. Furthermore, the $k$th product is equal to one, so the sum is equal to $y_k$ and the interpolation conditions are satisfied.

# CHAPTER FOUR
# NUMERICAL RESULTS

## 4.1 Exciton States in a Parabolic QD

### *4.1.1 Brief Overview*

Semiconductor quantum dots have been widely investigated in both theoretically (Hui, 2004; Banyain, & Koch, 1993; Woggon, 1997; Thao, & Viet, 2004; Ikezawa et. al., 2006; Loss, & DiVincenzo, 1998; Jaziri, & Bennaceur, 1995; Bruss, 1986) and experimentally (Johnson, & Payne, 1991; Hutton, 2004) in last a few decades. Quantum dots (QD) are low dimensional systems that well confined from all 3 spatial dimensions and in QDs (Hui, 2004) in which electrons and holes are fully quantized at separated energy levels. Powerful and effective optical properties of quantum dots make QDs important in the area of Optoelectronics and Nano-Device Development (Banyain, & Koch, 1993; Woggon, 1997;
Thao, & Viet, 2004). The binding energy of the excitonic systems is larger in QDs than in bulk material and, large binding energy of the biexciton state is important that such systems could be useful for operating a two-qubit gate in quantum computing (Ikezawa et. al., 2006; Loss, & DiVincenzo, 1998).

It is well known that excitonic systems have an important role to understand electronic and optical properties of QDs. There are wide range of works about the excitonic states in the QDs (Thao, & Viet, 2004; Jaziri, & Bennaceur, 1995; Bruss, 1986). The electron-hole interactions in small semiconductor crystals and electronic states depending on quantum dot size have been investigated by many researchers (Thao, & Viet, 2004; Bruss, 1986; Said, 1994). Electron systems under parabolic confinement are also attractive experimentally, dynamic and far infrared

responses of these systems have been studied (Wixforth et. al., 1994). To study of excitonic systems in terms of the quantum effects of their size is important in low dimensional QDs rather than the bulk semiconductors. The fabrication, size, shape and electronic properties of such systems can easily be controlled experimentally with the recent technologies (Tkach, & Seti, 2007). In our paper, the system has an electron and a light hole in GaAs quantum dot. Dynamical confinement by application of external field on electrons and holes implements of complete quantization of their free motion (Hu, & Lindberg, &, 1990) that make it possible to observe quantum size effect (QSE) in these quasi-zero-dimensional systems (Kayanuma, 1991).

Also, the ground state energy of an exciton in quantum dot with parabolic confinement has been investigated and the ground state energy data depending on quantum dot size has been studied (Said, 1994; Yildiz et. al., 2009). The excitonic binding energy in a quantum dot has been investigated via the variational method by converting the electron and hole coordinates to relative and center of mass coordinates and the ground state energy data depending on quantum dot size has been published (Thao, & Viet, 2004). Generally, infinite barriers have been considered as a confinement potential of excitons (Sakiroğlu et. al., 2009) and exact numerical solution of this system has been calculated by Hu, & Lindberg, & (1990). Parabolic potential profile is the basic model of this problem (Dempsey et. al., 1990) and this potential is suitable approach for a few electron QDs (Sikorski, & Merkt, 1989).

In our study, we used *Finite Element Method, (FEM)* for the numerical calculations of wave functions and quantized energy levels of exciton system in a parabolic quantum dot. The FEM, sometimes referred to as *finite element analysis, (FEA)*, is an effective computational technique used to obtain approximate solutions of boundary value problems in engineering, mathematics and physics (Hutton, 2004). In particular, the FEM represents

a stratagem of proven success for solving boundary value problems in quantum mechanics (Ram-Mohan, 2002). The FEM, used for calculating envelope functions and eigenvalues of $GaAs/AlGaAs$ and $InAs/GaSb$ quantum wells with arbitrary potential profiles in a high accuracy in the order of six ($10^{-6}$) is an effective method in the literature (Nakamura et. al., 1989).

Generally, only the ground state energy is calculated of exciton system in parabolic quantum dot using various different approximate methods in the literature as cited above. However, Li et. al. (2006) obtained the ground state energy, the first internal excited energy and the excitation energy in the strong-coupling polar crystal quantum dot as a function of the quantum dot radius. In this work, we computed the excited state energies of light hole exciton in parabolic quantum dot in a high accuracy in addition to the ground state.

In this chapter, we stated the exciton problem in parabolic quantum dot firstly, then expressed the application of FEM to the problem. Because of the system has a high spherical symmetry, we converted the coordinates of the electron hole system, explicitly reduce the dimension of the problem from 3D to 1D and used FEM via center of mass and relative coordinate. After that, we gave the numerical results for both ground state and excited state energy values of exciton. Finally, we showed the plots of the first 21 energy levels versus the confinement parameter and the interaction parameter depending on infinite quantum dot size in 3D and in two different energy scales.

### *4.1.2 Theory and Method*

Simply, the bounded states of an electron and hole called exciton. In the literature, this two-body system has been investigated to understand the electronic properties of quantum dots in different ways (Banyain, & Koch, 1993;

Woggon, 1997). The Hamiltonian of such system in spherical quantum dot under a parabolic confinement;

$$\mathcal{H} = \mathcal{H}_1 + \mathcal{H}_2 + \mathcal{V}_{12} \tag{4.1.1}$$

$$\mathcal{H}_i = -\frac{\hbar^2}{2m_i}\vec{\nabla}_i^2 + V_i(\vec{r}_i) \tag{4.1.2}$$

$(i = 1, 2)$ here for electron and hole respectively and the interaction term is Coulombic;

$$\mathcal{V}_{12} = \frac{-e^2}{4\pi\epsilon r} \tag{4.1.3}$$

Equation (4.1.2) represents the independent Hamiltonian of two particles. Here, we took the confinement potentials like harmonic oscillators which oscillating with the same frequency $w$. Assumption of identical parabola frequency for the different charge carriers indicates that the range of electron and hole potentials are approximately the same. This is not a bad approximation for the materials like GaAs (Garm, 1996). Therefore it is expected to have great overlap between electron and hole wave functions and strong Coulomb interaction.

$$V_i(\vec{r}_i) = \frac{1}{2}m_i w^2 \vec{r}_i^2 \tag{4.1.4}$$

We considered the relative coordinate between the particles ($\vec{r}$) and center of mass coordinate ($\vec{R}$) of particles for numerical solutions instead of solving the system via electron and hole coordinates directly in spherical parabolic quantum dot. By using these variables, we write down the total mass Hamiltonian and interaction Hamiltonian as

$$\mathcal{H} = \left(-\frac{\hbar^2}{2M}\vec{\nabla}_{\vec{R}}^2 + \frac{1}{2}Mw^2\vec{R}^2\right) \tag{4.1.5}$$

$$+\left(-\frac{\hbar^2}{2\mu}\vec{\nabla}^2_{\vec{r}}+\frac{1}{2}\mu w^2\vec{r}^2-\frac{e^2}{4\pi\epsilon}\frac{1}{\vec{r}}\right)$$

$$\mathcal{H}=\mathcal{H}_R+\mathcal{H}_r$$

Here, $\mu$ and $M$ are the reduced mass and total mass of the system, respectively. Equation (4.1.5) should be made dimensionless before the numerical calculations. We consider it as two parts: relative and center of mass. These equations can be made dimensionless by using $\hbar w$ or effective Hartree energy ($\varepsilon_h^*$) scale.

In $\hbar w$ energy regime, we choose the magnetic length $l_\mu=\sqrt{\frac{\hbar}{\mu w}}$ as the length scale. Thus, the coordinates replaces as follows, $R\rightarrow l_\mu R$ and $r\rightarrow l_\mu r$. Therefore total mass and interaction Hamiltonians become

$$\frac{\mathcal{H}_R}{\hbar w}=\left(\frac{\mu}{M}\right)\left(-\frac{1}{2}\vec{\nabla}^2_{\vec{R}}+\frac{1}{2}\left(\frac{M}{\mu}\right)^2\vec{R}^2\right) \tag{4.1.6}$$

and

$$\frac{\mathcal{H}_r}{\hbar w}=\left(-\frac{1}{2}\vec{\nabla}^2_{\vec{r}}+\frac{1}{2}\vec{r}^2-\frac{W_\mu^{-1/2}}{r}\right) \tag{4.1.7}$$

Here we define $\kappa=\frac{l_\mu}{a_B^*}$ as the interaction parameter with effective Bohr radius $a_B^*=\frac{4\pi\epsilon\hbar^2}{\mu e^2}$. In Equation (4.1.7), $W_\mu$ is the confinement parameter and the relation between the interaction parameter and confinement parameter is $W_\mu^{-1/2}=\kappa$. In effective Bohr energy ($\varepsilon_h^*$) regime we choose the effective Bohr radius as the length scale. Similarly, the coordinates replaces as follows, $R\rightarrow a_B^*R$ and $r\rightarrow a_B^*r$. Therefore total mass and interaction

Hamiltonians become

$$\frac{\mathcal{H}_R}{\varepsilon_h^*}=\left(\frac{\mu}{M}\right)\left(-\frac{1}{2}\vec{\nabla}^2_{\vec{R}}+\frac{1}{2}\left(\frac{M}{\mu}\right)^2W_\mu^2\vec{R}^2\right) \tag{4.1.8}$$

and

$$\frac{\mathcal{H}_r}{\varepsilon_h^*} = \left( -\frac{1}{2}\vec{\nabla}_{\vec{r}}^2 + \frac{1}{2}W_\mu^2\vec{r}^2 - \frac{1}{r} \right) \tag{4.1.9}$$

### *4.1.3 General Formalism of Finite Element Method and High Symmetry*

In generally the dimensionless Hamiltonian of one particle under a general potential profile $V(r)$ is,

$$\mathcal{H} = -\frac{1}{2}\vec{\nabla}^2 + V(r) \tag{4.1.10}$$

This expression is in the type of single particle Hamiltonian under $V(r)$ potential profile and it is possible to reduce the dimension of the problem to 1D because of the high spherical symmetry instead of calculating the eigenvalues and eigenvectors in 3D. Equations (4.1.6), (4.1.7), (4.1.8) and (4.1.9) are in the form of Equation (4.1.10). Before writing the Hamiltonian, let us mention about the minimization in Finite Element Method. Forming the work space with appropriate basis set should be the first step of the numerical calculations. According to this, we expand the wave function with a basis set by serial expansion and search the variable parameters which amount of them is equal to the number of nodes. In this paper, we applied *Galerkin Method* (Kwon, & Bang, 2000) as the minimization method to the problem. We used the separation of variables because of the Spherical Harmonics is orthanormal and we can

constitute the $G$ expression in equation (13) depending on only radial variable $r$. This is, namely, reducing the dimension of the problem that in 3D to 1D and then, we had the FEM solutions via radial variable over the whole workspace. If we write the Equation (4.1.10) with spherical coordinates,

$$\mathcal{H} = -\frac{1}{2}\left( \frac{1}{r^2}\frac{d}{dr}r^2\frac{d}{dr} - \frac{l(l+1)}{r^2} \right) + V(r) \tag{4.1.11}$$

and this equation needs to be solved;

$$\mathcal{H}\psi(r) = \varepsilon\psi(r). \tag{4.1.12}$$

The $G$ expression as mentioned above is

$$G = \int_0^\infty dr r^2 \psi(r)^\dagger (\mathcal{H} - \varepsilon)\psi(r). \tag{4.1.13}$$

Thus it becomes

$$G = \int_0^\infty dr \psi(r)^\dagger \left[ -\frac{1}{2}\frac{d}{dr} r^2 \frac{d}{dr} + \left( \frac{l(l+1)}{2} \right) \right. \tag{4.1.14}$$

$$\left. + r^2 (V(r) - \varepsilon) \right] \psi(r).$$

The $(\psi, \psi^\dagger)$ family which minimize equation (4.1.14) is the exact wave function that gives the exact solution. We used a serial expansion of the radial function with number of nodes $(N)$ of the work space and the basis functions $(\mathbb{N}_n(r))$ in the same work space.

$$\psi(r) = \sum_{n=1}^{N} \psi_n \mathbb{N}_n(r) \tag{4.1.15}$$

The matrix form of equation (4.1.14) is

$$\begin{aligned} \psi(r) &= \bar{\mathbb{N}}^T \bar{\psi} \\ \psi^\dagger(r) &= \bar{\psi}^\dagger \bar{\mathbb{N}}. \end{aligned} \tag{4.1.16}$$

After that, by using the principle of variation to reach the solution the

*Generalized Eigenvalue Equation* is constructed which is,

$$\frac{\partial G}{\partial \bar{\psi}^{\dagger}} = 0 \tag{4.1.17}$$

Thus we get, in matrix form;

$$\bar{\bar{K}}\bar{\psi} = \varepsilon \bar{\bar{M}}\bar{\psi}. \tag{4.1.18}$$

Here, $\bar{\bar{K}}$ and $\bar{\bar{M}}$ called as Stiffness Matrix and Mass Matrix, respectively. According to the boundary conditions, the solutions should decay at the boundaries of the system. If we consider the boundary conditions and the fact that the integrals over the whole work space could be written as the summation of the integrals over the global elements $\Omega_i$, we write the Stiffness and Mass matrices,

$$\bar{\bar{K}} = \sum_{i=1}^{N_e} \left[ \frac{1}{2} \left( \int_{\Omega_i} dr r^2 \frac{d\bar{\mathbb{N}}}{dr} \frac{d\bar{\mathbb{N}}^T}{dr} \right) + \left( \frac{l(l+1)}{2} \right) \left( \int_{\Omega_i} dr \bar{\mathbb{N}}\bar{\mathbb{N}}^T \right) \right. \tag{4.1.19}$$

$$\left. + \left( \int_{\Omega_i} dr (r^2 V(r)) \bar{\mathbb{N}}\bar{\mathbb{N}}^T \right) \right]$$

$$\bar{\bar{M}} = \sum_{i=1}^{N_e} \left( \int_{\Omega_i} dr r^2 \bar{\mathbb{N}}\bar{\mathbb{N}}^T \right) \tag{4.1.20}$$

Here $N_e$ is the number of global elements and $\bar{\mathbb{N}}$ is the matrix form of global element basis function.

### *4.1.4 Results and Conclusion of The Exciton Problem*

In this chapter, we give the numerical results of exciton in parabolic QD. We took $m_e = 0.067m_0$ and $m_h = 0.40m_0$ as the masses of the particles in order to solve the Equations (4.1.6), (4.1.7), (4.1.8) and (4.1.9) numerically. We gave the first 21 energy levels of exciton in $\hbar w$ scala in Table 4.1. These values are total energies that calculated from Equation (4.1.6) and (4.1.7), and sorted for $W_\mu^{(-1/2)} = 1.0$. Here, $(N, L)$ represent the principal and angular momentum quantum numbers respectively for center of mass part and $(n, l)$ represent the same numbers for the relative part. The energy values have high accuracy because of FEM as one can see in Table 4.1. In Figure 4.1, the energy spectra that contains first 21 levels given in Table 4.1 depending on $W_\mu^{-1/2}$ is shown. Here, the values on the left ordinate (for $W_\mu^{-1/2} = 0.0$) are the total values of Harmonic Oscillator problem in 3D as expected with high accuracy. Besides, Equation (4.1.6) and (4.1.7) transform the Harmonic Oscillator type Hamiltonians with this value of $W_\mu^{-1/2}$. The values start from $3.0\hbar w$ and increase with an integer number. It is interesting that the number of lines for first energy, $3.0\hbar w$, is one, the second energy, $4.0\hbar w$, is two, and so on. It should be noted that the crossing occurs for different $W_\mu^{-1/2}$ values showed in Figure 4.1. Table 4.2 contains first 21 energy values of exciton in Effective Hartree energy scala for $W_\mu = 0.05$ that is in Equation (4.1.8) and (4.1.9). Here $(N, L; n, l)$ have the similar meaning as mentioned above. Figure 4.2 shows the energy spectra of exciton in parabolic QD of first 21 levels in Effective Hartree energy scala depending on confinement parameter $W_\mu$. The values for $W_\mu = 0.0$ are the energies of Hydrogen atom problem that can be seen in the left ordinate of Figure 4.2. Equation (4.1.8) and (4.1.9) become Hydrogen atom Hamiltonian for this value of $W_\mu$. In the calculations to get the energy values given in Table 4.1 and Table 4.2, we took the relative distance between electron and hole as $r = 10l_\mu$ and $r = 10a_B^*$ for $\hbar w$ and Effective Hartree regime, respectively. This work space contains 57 global elements and we use 8th order of interpolating functions in every global element

for Finite Element calculations. There are 400 nodes in whole workspace.

Here, we obtained the solutions of an exciton problem in a parabolic QD with high accuracy ($10^{-9}$) by using FEM. If one wants to get higher accuracy, it can be done with more nodes in the workspace and higher order of interpolating functions in global elements under some numerical limits. FEM is very strong and effective method which gives us higher excited states with high accuracy in quite small computation time. The computation time is nearly a few seconds for one quantum dot size. In our work, we showed the exact numerical calculations and results of the exciton system in spherical parabolic quantum dot using Finite Element Method. Firstly, we convert the coordinates of the electron and hole system to relative and center of mass coordinates, namely, reduce the dimension of the problem from 3D to 1D which is done by the high spherical symmetry, thus we were able to use Finite Element Method to only radial variable. This method gives the exact numerical solutions for the Harmonic Oscillator as in shown in Figure 4.1 for $W_{\mu}^{-1/2} = 0.0$ and Hydrogen Atom problems as in shown in Figure 4.2 for $W_{\mu} = 0.0$.

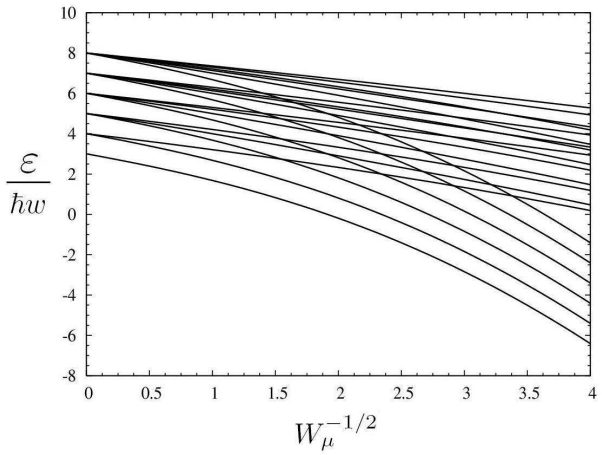


Figure 4.1 Energy Spectrum of exciton in $\hbar w$ units. First 21 level is shown. Sorted for $W_\mu^{-1/2} = 1.0$ as in Table 1.

Table 4.1 First 21 energy values of an exciton in 3D spherical parabolic QD. Energies are in $\hbar w$ units.

| | $(N, L; n, l)$ | $W_\mu^{(-1/2)} = 1.0$ |
|---|---|---|
| 1 | (0,0;0,0) | 1.6796684846 |
| 2 | (0,1;0,0) | 2.6796684846 |
| 3 | (0,0;0,1) | 3.2090180911 |
| 4 | (1,0;0,0) | 3.6796684846 |
| 5 | (0,0;1,0) | 3.9999999999 |
| 6 | (0,1;0,1) | 4.2090180911 |
| 7 | (1,1;0,0) | 4.6796684846 |
| 8 | (0,1;1,0) | 5.0000000000 |
| 9 | (1,0;0,1) | 5.2090180911 |
| 10 | (0,0;1,1) | 5.3019296096 |
| 11 | (2,0;0,0) | 5.6796684846 |
| 12 | (1,0;1,0) | 6.0000000000 |
| 13 | (0,0;2,0) | 6.1319524088 |
| 14 | (1,1;0,1) | 6.2090180911 |
| 15 | (0,1;1,1) | 6.3019296096 |
| 16 | (2,1;0,0) | 6.6796684846 |
| 17 | (1,1;1,0) | 7.0000000000 |
| 18 | (0,1;2,0) | 7.1319524088 |
| 19 | (2,0;0,1) | 7.2090180911 |
| 20 | (1,0;1,1) | 7.3019296096 |
| 21 | (0,0;2,1) | 7.3603571728 |

Table 4.2 First 21 energy values of an exciton in 3D spherical parabolic QD. Energies are in $\varepsilon_h^*$ units.

| | $(N, L; n, l)$ | $W_\mu = 0.05$ |
|---|---|---|
| 1 | (0,0;0,0) | -0.4148695530 |
| 2 | (0,1;0,0) | -0.3510523498 |
| 3 | (1,0;0,0) | -0.2580759132 |
| 4 | (1,1;0,0) | -0.1540169759 |
| 5 | (0,0;0,1) | -0.0122734066 |
| 6 | (2,0;0,0) | -0.0105961913 |
| 7 | (0,0;1,0) | 0.0022629450 |
| 8 | (0,1;0,1) | 0.0515437965 |
| 9 | (0,1;1,0) | 0.0660801482 |
| 10 | (2,1;0,0) | 0.1411657160 |
| 11 | (1,0;0,1) | 0.1445202331 |
| 12 | (1,0;1,0) | 0.1590565849 |
| 13 | (0,0;1,1) | 0.1757569101 |
| 14 | (0,0;2,0) | 0.2206579060 |
| 15 | (0,1;1,1) | 0.2395741133 |
| 16 | (1,1;0,1) | 0.2485791705 |
| 17 | (1,1;1,0) | 0.2631155222 |
| 18 | (0,1;2,0) | 0.2844751092 |
| 19 | (1,0;1,1) | 0.3325505500 |
| 20 | (3,0;0,0) | 0.3349300628 |
| 21 | (1,0;2,0) | 0.3774515459 |

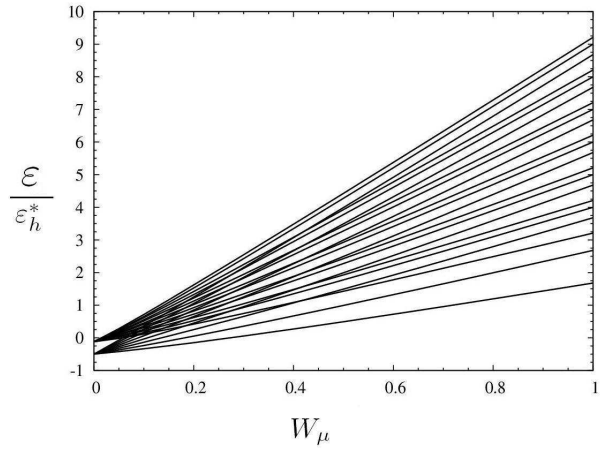


Figure 4.2 Energy Spectrum of exciton in Effective Hartree Energy units. First 21 level is shown. Sorted for $W_\mu = 0.05$ as in Table 2.

## 4.2 Free Particle in Quantum Wires (2D)

### *4.2.1 Generalized Eigen-Value Problem with Interpolating Polynomial and Matrix Elements*

We have mention about how to derive the Generalized Eigen Value equation in section 3.2.2. of this thesis. Here, we start the generalized eigen value equation;

$$\{\{K\}\}\{\psi\} = \varepsilon\{\{M\}\}\{\psi\} \tag{4.2.1}$$

$$\{\{M\}\} = \int_{\Omega} d\Omega\{\phi(x)\}\{\phi(x)\}^T \tag{4.2.2}$$

Here,

$$x = (x_1, x_2, ..., x_d)$$

$$d\Omega = \prod_{i=1}^{d} dx_i$$

Similarly, for the Stiffness matrix,

$$\{\{K\}\} = \int_{\Omega} d\Omega \left[\frac{\hbar^2}{2m^*}\vec{\nabla}\{\phi(x)\}\vec{\nabla}\{\phi(x)\}^T + \{\phi(x)\}V(x)\{\phi(x)\}^T\right] \tag{4.2.3}$$

Here,

$$\Omega = \sum_{e=1}^{N_e} \Omega_e$$

$$\{\phi(x)\} \rightarrow \text{Whole Work Space Basis}$$

$$\{N(x)\} \rightarrow \text{Global Element Basis}$$

After the scaling with effective Hartree energy,

$$E_h^* = \frac{\hbar^2}{m^*(a^*)^2} = \frac{e^2}{4\pi\epsilon}\frac{1}{a^*} \tag{4.2.4}$$

$$\vec{r} \rightarrow a^*\vec{r}$$

$$V \rightarrow E_h^* V$$

$$E \rightarrow E_h^* E$$

Therefore Equation (4.2.3) becomes

$$\{\{K\}\} = \int_\Omega d\Omega \left[\frac{1}{2}\vec{\nabla}\{\phi(x)\}\vec{\nabla}\{\phi(x)\}^T + \{\phi(x)\}V(x)\{\phi(x)\}^T\right] \tag{4.2.5}$$

These integrals over the whole work space can be written as summation of the integrals ever the global elements. Thus,

$$\{\{M\}\} = \sum_{e=1}^{N_e}\int_{\Omega_e} d\Omega_e\{N(x)\}\bar{\{N(x)\}}^T \tag{4.2.6}$$

$$\{\{m_e\}\} = \int_{\Omega_e} d\Omega_e\{N(x)\}\{N(x)\}^T \tag{4.2.7}$$

and

$$\{\{M\}\} = \sum_{e=1}^{N_e}\{\{m_e\}\} \tag{4.2.8}$$

Similarly,

$$\{\{k_e\}\} = \{\{k_{e,kin}\}\} + \{\{k_{e,pot}\}\}$$

$$\{\{k_{e,kin}\}\} = \int_{\Omega_e} d\Omega_e \left[\frac{1}{2}\vec{\nabla}\{N(x)\}\vec{\nabla}\{N(x)\}^T\right] \tag{4.2.9}$$

$$\{\{k_{e,pot}\}\} = \int_{\Omega_e} d\Omega_e \left[\{N(x)\}V(x)\{N(x)\}^T\right] \tag{4.2.10}$$

$$\{\{K\}\} = \sum_{e=1}^{N_e} \{\{k_e\}\} \tag{4.2.11}$$

$$d\Omega_e = \prod_{i=1}^{d} dx_i$$

$$\{N(x)\}^T = \begin{pmatrix} N_1(x) & N_2(x) & \cdots & N_{d+1}(x) \end{pmatrix}$$

$$d\Omega_e = J_e \quad dL_1 dL_2 \cdots dL_d$$

Therefore, the matrix elements for the global element mass matrix $m_e$,

$$\begin{pmatrix} m_e \end{pmatrix}_{ij} = J_e \int_0^1 dL_1 \int_0^{1-L_1} dL_2 \int_0^{1-L_1-L_2} dL_3 \quad \cdots \tag{4.2.12}$$

$$\cdots \int_0^{1-L_1-L_2-\cdots-L_{d-1}} dL_d \quad N_i(L)N_j(L)$$

$$L = (L_1, l_2, \cdots, L_d, L_{d+1})$$

The matrix elements of the potential part for the global element stiffness matrix $k_{e,pot}$,

$$\{\{k_{e,pot}\}\} = \int_{\Omega_e} d\Omega_e \left[\{N(x)\}V(x)\{N(x)\}^T\right]$$

If $N_{\text{gen}} \rightarrow$ global element node number

$$V(x) = \sum_{e=1}^{N_{\text{gen}}} V_i \cdot N_i(x) \tag{4.2.13}$$

$$\left( \ k_{e,pot} \ \right)_{ij} = \sum_{k=1}^{N_{\text{gen}}} V_k \cdot \quad J_e \int_0^1 dL_1 \quad \int_0^{1-L_1} dL_2 \quad \int_0^{1-L_1-L_2} dL_3 \quad \cdots \tag{4.2.14}$$

$$\cdots \quad \int_0^{1-L_1-L_2-\cdots-L_{d-1}} dL_d \quad N_i(L) N_k(L) N_j(L)$$

The matrix elements of the potential part for the global element stiffness matrix $k_{e,kin}$;

$$\{\{k_{e,kin}\}\} = \int_{\Omega_e} d\Omega_e \left[ \frac{1}{2} \vec{\nabla}\{N(x)\} \vec{\nabla}\{N(x)\}^T \right]$$

$$\vec{\nabla}\{N(x)\} \vec{\nabla}\{N(x)\}^T = \sum_{i=1}^{d} \frac{\partial\{N(x)\}}{\partial x_i} \frac{\partial\{N(x)\}^T}{\partial x_i}$$

$$\{\{k_{e,kin}\}\} = \sum_{i=1}^{d} \int_{\Omega_e} d\Omega_e \frac{1}{2} \left( \frac{\partial\{N(x)\}}{\partial x_i} \right) \left( \frac{\partial\{N(x)\}^T}{\partial x_i} \right)$$

Here,

$$\frac{\partial\{N(x)\}}{\partial x_i} = \begin{pmatrix} \frac{\partial N_1}{\partial x_i} \\ \frac{\partial N_2}{\partial x_i} \\ \frac{\partial N_3}{\partial x_i} \\ \vdots \\ \frac{\partial N_{N_{gen}}}{\partial x_i} \end{pmatrix} = \sum_{j=1}^{d} \left( \frac{\partial L_j}{\partial x_i} \right) \left( \frac{\partial\{N\}}{\partial L_j} \right)$$

Similarly,

$$\frac{\partial\{N(x)\}^T}{\partial x_i} = \sum_{k=1}^{d} \left( \frac{\partial L_k}{\partial x_i} \right) \left( \frac{\partial\{N\}^T}{\partial L_k} \right)$$

$$\{\{k_{e,kin}\}\} = \sum_{i=1}^{d} \sum_{j=1}^{d} \sum_{k=1}^{d} \int_{\Omega_e} d\Omega_e \frac{1}{2} \left( \frac{\partial L_j}{\partial x_i} \frac{\partial\{N\}}{\partial L_j} \right) \left( \frac{\partial L_k}{\partial x_i} \frac{\partial\{N\}^T}{\partial L_k} \right)$$

$$= \sum_{i=1}^{d}\sum_{j=1}^{d}\sum_{k=1}^{d} \frac{1}{2}\left(\frac{\partial L_j}{\partial x_i}\right)\left(\frac{\partial L_k}{\partial x_i}\right)\cdot J_e\cdot$$

$$\cdot\int_0^1 dL_1 \int_0^{1-L_1} dL_2 \int_0^{1-L_1-L_2} dL_3 \cdots \int_0^{1-L_1-L_2-\cdots-L_{d-1}} dL_d \left(\frac{\partial\{N(L)\}}{\partial L_j}\right)\left(\frac{\partial\{N(L)\}^T}{\partial L_k}\right)$$

Therefore,

$$\left( k_{e,kin} \right)_{lm} = \sum_{i=1}^{d}\sum_{j=1}^{d}\sum_{k=1}^{d} \frac{1}{2}\left(\frac{\partial L_j}{\partial x_i}\right)\left(\frac{\partial L_k}{\partial x_i}\right)\cdot J_e\cdot \tag{4.2.15}$$

$$\cdot\int_0^1 dL_1 \int_0^{1-L_1} dL_2 \int_0^{1-L_1-L_2} dL_3 \cdots \int_0^{1-L_1-L_2-\cdots-L_{d-1}} dL_d \left(\frac{\partial N_l(L)}{\partial L_j}\right)\left(\frac{\partial N_m^T(L)}{\partial L_k}\right)$$

Here, $J_e$ is the volume element of the global element.

### *4.2.2 Numerical Results*

In this section, there will be the numerical results calculated with the equations which in previous sections. The single particle solutions and the solutions with potential profiles are presented for six different quantum wire cross-sections. The numerical solutions are controlled and tested with the analytical solutions of the known problems such as single particle in square quantum wire which in next section.

### *4.2.3 Square Quantum Wire*

Figure 4.3 shows a uniform square mesh. Here, the boundaries which on the potential is infinity are indicated little circles thats color are red. The length of

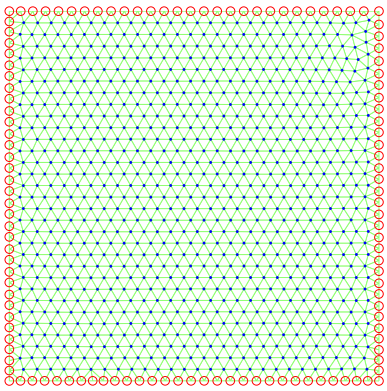

Figure 4.3 A uniform mesh for the problem single particle in square quantum wire.

the edges of the square is $4a^*$ (four effective Bohr radious). The other features of the mesh can be given as: Number of triangular elements: 1797, Number of total vertices : 961, Number of BOUNDARY vertices : 123, Number of INNER vertices : 838, Min quality : 0.64533, Uniformity : 1.694. Figure 4.4 to Figure 4.12 show us the localizations of the charged particle in square quantum wire for no potential, parabolic potential and linear potential profiles. Table 4.3 relates the figure names, confinement profiles, excited numbers and the energies of the single particle problem in square quantum wire. For being sure about the numerical solutions in Table 4.3 are correct, we should mention about the analytical solution of this problem. The analytical solution of the single particle quantum wire is;

$$\varepsilon_{n_x,n_y} = \frac{1}{L^2}(n_x^2 + n_y^2). \tag{4.2.16}$$

Here, $L$ is the length of the quantum wire. $n_x$ and $n_y$ are the principal quantum numbers of the system which considered in $xy-$ plane.

Table 4.3 The information table for the problem known as one particle in square quantum wire. Energies are $E_h^*$ units. The inner node numbers are shown in parenthesis in last two column.

| Fig. Label | Confinement | State Number | En. (407) | En. (7145) |
|---|---|---|---|---|
| 4.4 | No | Ground State | 0.12541 | 0.12502 |
| 4.5 | Parabolic | Ground State | 0.61225 | 0.60819 |
| 4.6 | Linear | Ground State | 0.47832 | 0.47738 |
| 4.7 | No | 1st Excited | 0.31503 | 0.31265 |
| 4.8 | Parabolic | 1st Excited | 1.02264 | 1.01410 |
| 4.9 | Linear | 1st Excited | 0.70096 | 0.69807 |
| 4.10 | No | 2nd Excited | 0.31515 | 0.31265 |
| 4.11 | Parabolic | 2nd Excited | 1.02446 | 1.01420 |
| 4.12 | Linear | 2nd Excited | 0.70141 | 0.69810 |

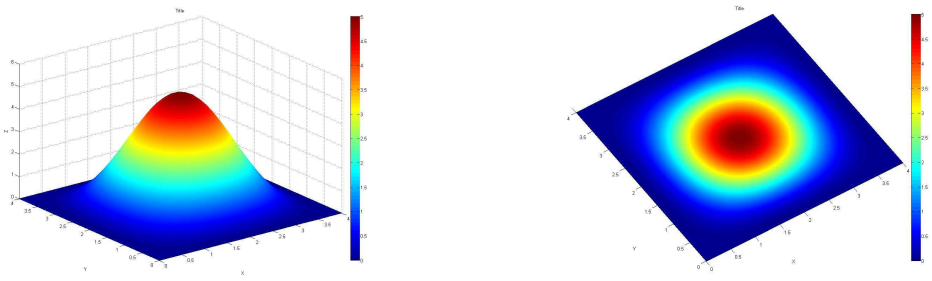

(a) (b)

Figure 4.4 Ground State charge localization of a single particle in square quantum wire with no potential profile. (a) General view (b) from the top view.

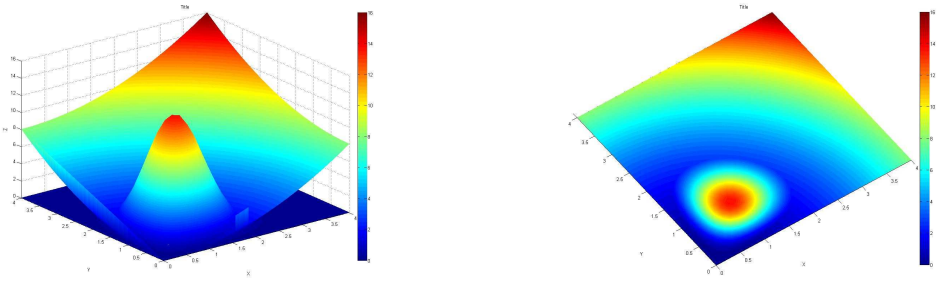

(a) (b)

Figure 4.5 Ground State charge localization of a single particle in square quantum wire with parabolic potential profile. (a) General view (b) from the top view.

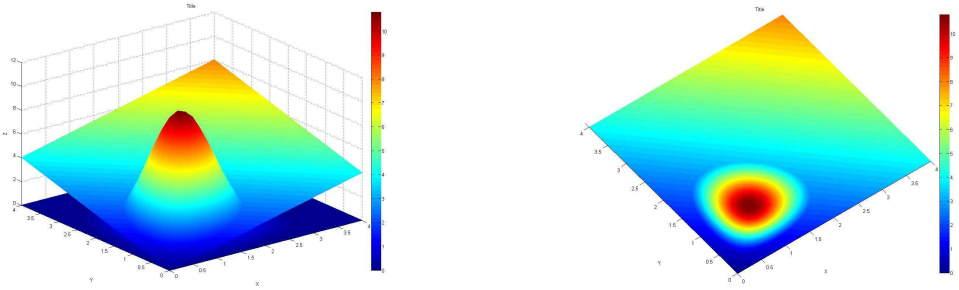

(a) (b)

Figure 4.6 Ground State charge localization of a single particle in square quantum wire with linear potential profile. (a) General view (b) from the top view.

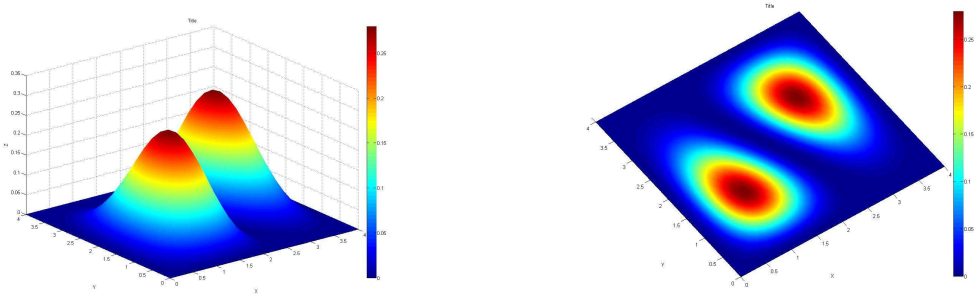

(a) (b)

Figure 4.7 First Excited State charge localization of a single particle in square quantum wire with no potential profile. (a) General view (b) from the top view.

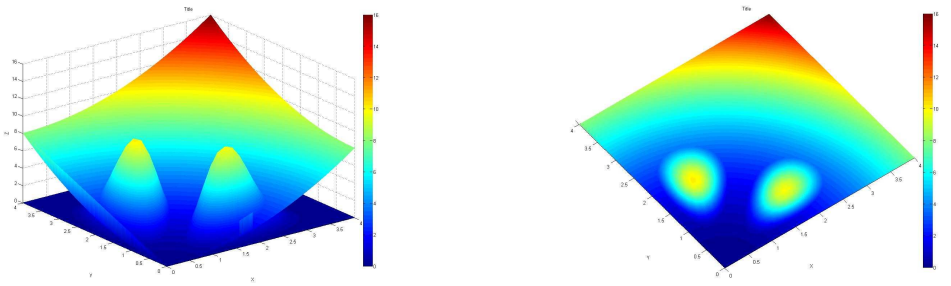

(a) (b)

Figure 4.8 First Excited State charge localization of a single particle in square quantum wire with parabolic potential profile. (a) General view (b) from the top view.

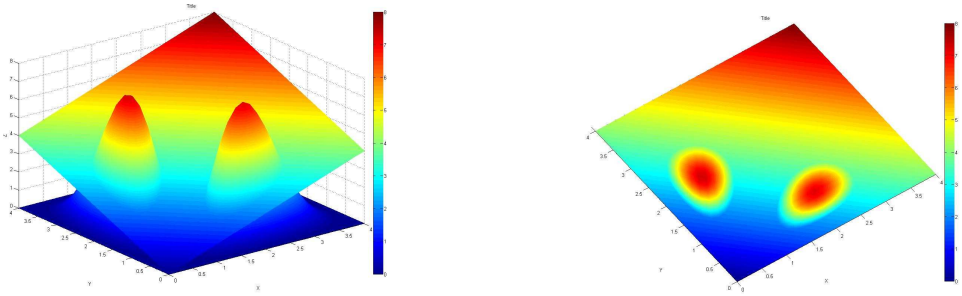

(a) (b)

Figure 4.9 First Excited State charge localization of a single particle in square quantum wire with linear potential profile. (a) General view (b) from the top view.

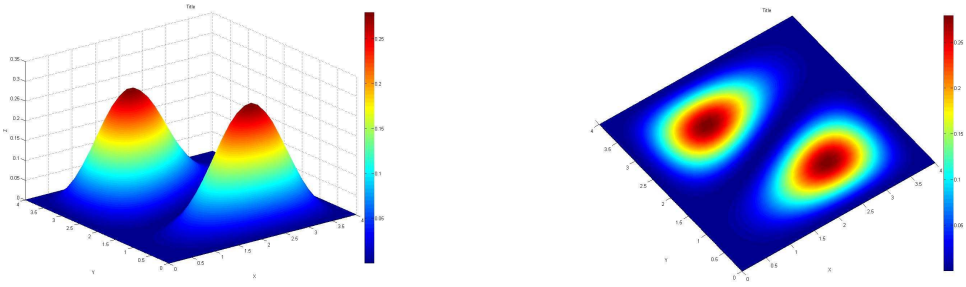

(a) (b)

Figure 4.10 Second Excited State charge localization of a single particle in square quantum wire with no potential profile. (a) General view (b) from the top view.

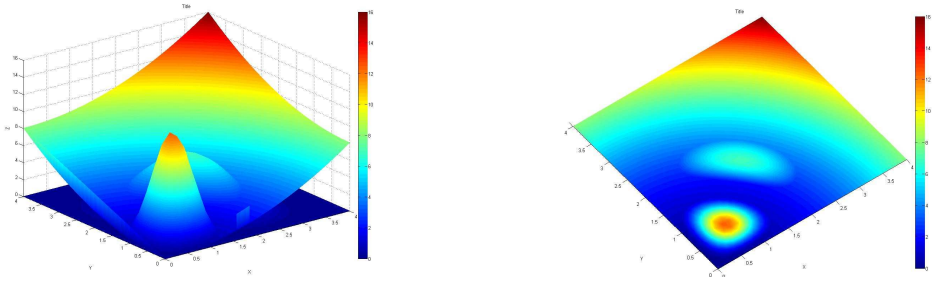

(a) (b)

Figure 4.11 Second Excited State charge localization of a single particle in square quantum wire with parabolic potential profile. (a) General view (b) from the top view.

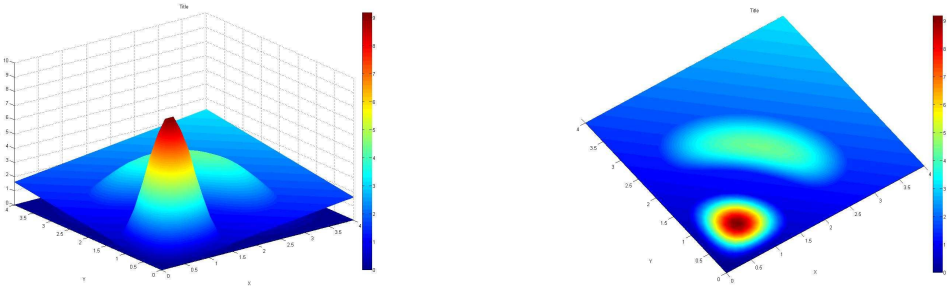

(a) (b)

Figure 4.12 Second Excited State charge localization of a single particle in square quantum wire with linear potential profile. (a) General view (b) from the top view.

### *4.2.4 Triangular Quantum Wire*

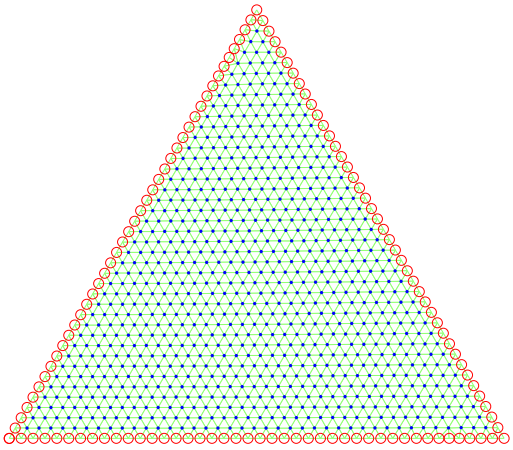

Figure 4.13 A uniform mesh for the problem single particle in triangular quantum wire.

Figure 4.13 shows a uniform mesh for a triangular work space. Here again, the boundaries which on the potential is infinity are indicated little circles thats color are red. The length of the edges of the triangle is $1a^*$ (one effective Bohr radious). The other features of the mesh can be given as: Number of triangular elements: 1683, Number of total vertices: 906 Number of BOUNDARY vertices: 126, Number of INNER vertices: 780, Min quality: 0.78933, Uniformity: 0.94353. Figure 4.14 to Figure 4.22 show us the localizations of the charged

particle in triangular quantum wire for no potential, parabolic potential and linear potential profiles. Table 4.4 relates the figure names, confinement profiles, excited numbers and the energies of the single particle problem in triangular quantum wire, similarly as in the previous the section for the square quantum wire.

Table 4.4 The information table for the problem known as one particle in triangular quantum wire. Energies are $E_h^*$ units. The inner node numbers are shown in parenthesis in last two column.

| Fig. label | Confinement | State Number | En. (536) | En. (4697) |
|---|---|---|---|---|
| 4.14 | No | Ground State | 5.34874 | 5.33517 |
| 4.15 | Parabolic | Ground State | 5.38518 | 5.37159 |
| 4.16 | Linear | Ground State | 5.43143 | 5.41787 |
| 4.17 | No | 1st Excited | 12.52804 | 12.45443 |
| 4.18 | Parabolic | 1st Excited | 12.55927 | 12.48533 |
| 4.19 | Linear | 1st Excited | 12.60148 | 12.52756 |
| 4.20 | No | 2nd Excited | 12.52836 | 12.45444 |
| 4.21 | Parabolic | 2nd Excited | 12.57461 | 12.50099 |
| 4.22 | Linear | 2nd Excited | 12.62035 | 12.54675 |

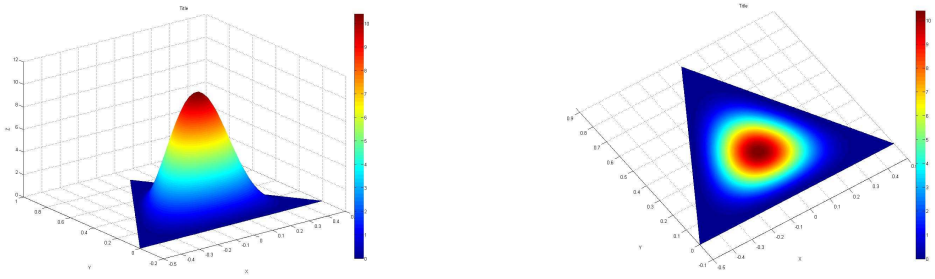

(a) (b)

Figure 4.14 Ground State charge localization of a single particle in triangular quantum wire with no potential profile. (a) General view (b) from the top view.

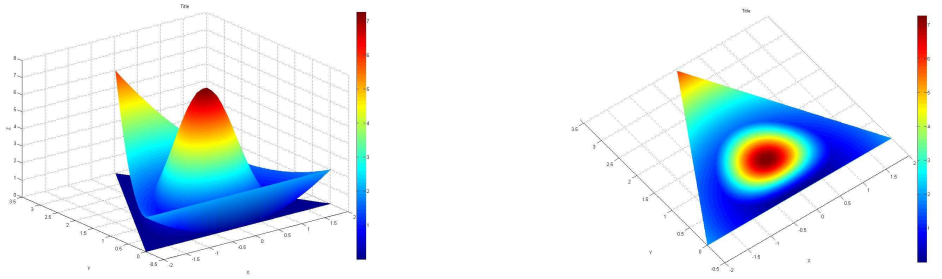

(a) (b)

Figure 4.15 Ground State charge localization of a single particle in triangular quantum wire with parabolic potential profile. (a) General view (b) from the top view.

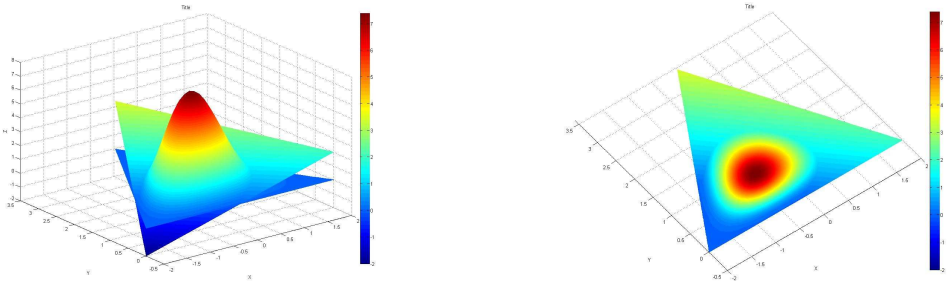

(a) (b)

Figure 4.16 Ground State charge localization of a single particle in triangular quantum wire with linear potential profile. (a) General view (b) from the top view.

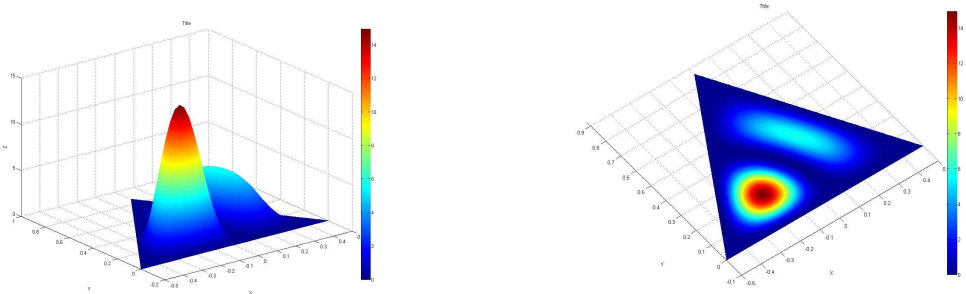

(a) (b)

Figure 4.17 First Excited State charge localization of a single particle in triangular quantum wire with no potential profile. (a) General view (b) from the top view.

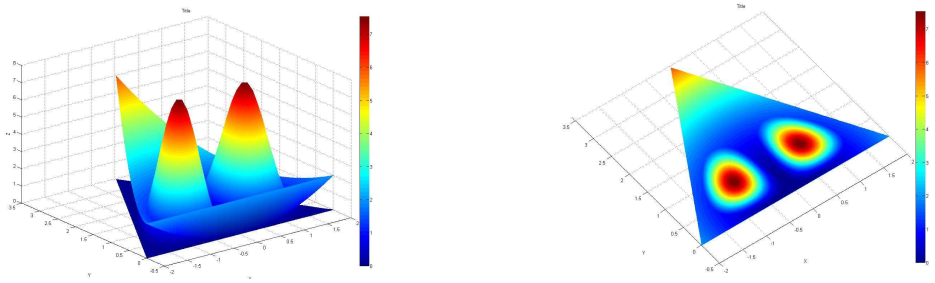

(a) (b)

Figure 4.18 First Excited State charge localization of a single particle in triangular quantum wire with parabolic potential profile. (a) General view (b) from the top view.

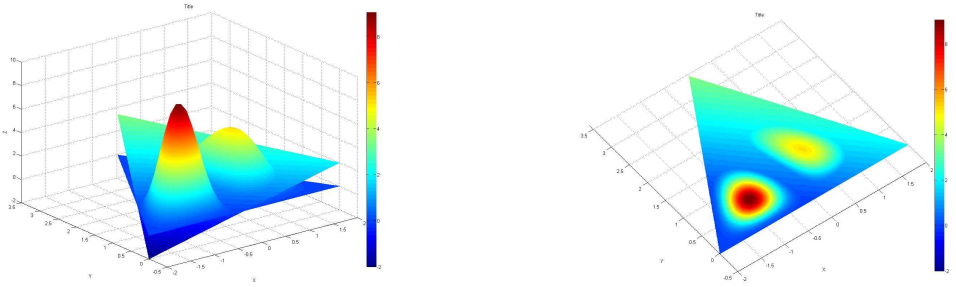

(a) (b)

Figure 4.19 First Excited State charge localization of a single particle in triangular quantum wire with linear potential profile. (a) General view (b) from the top view.

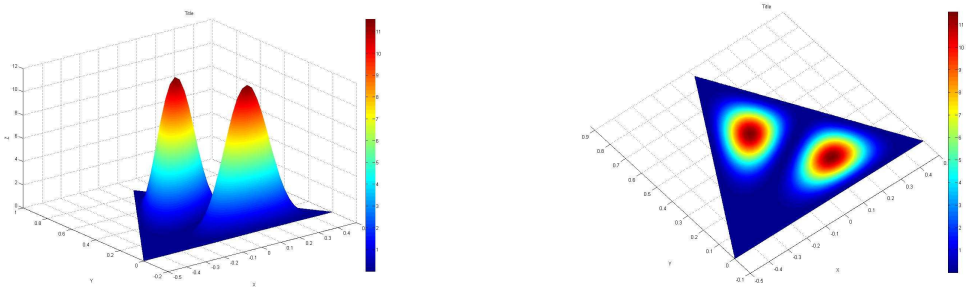

(a) (b)

Figure 4.20 Second Excited State charge localization of a single particle in triangular quantum wire with no potential profile. (a) General view (b) from the top view.

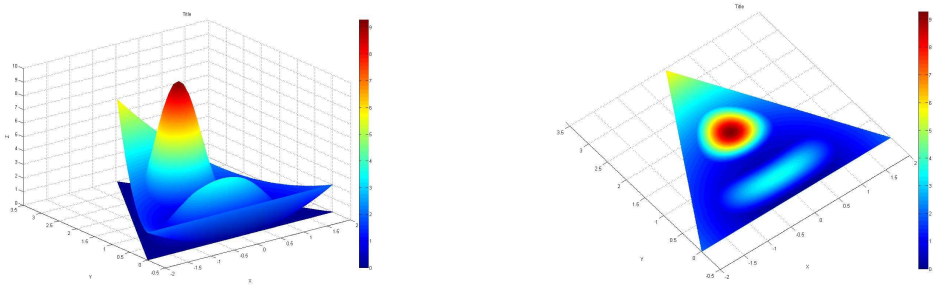

(a) (b)

Figure 4.21 Second Excited State charge localization of a single particle in triangular quantum wire with parabolic potential profile. (a) General view (b) from the top view.

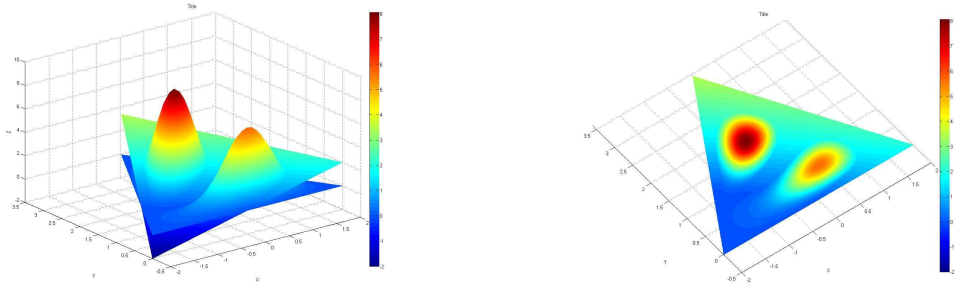

(a) (b)

Figure 4.22 Second Excited State charge localization of a single particle in triangular quantum wire with linear potential profile. (a) General view (b) from the top view.

Figure 4.23 shows us the ground state localizations of six different quantum wire cross-sections. The caption of this figure has the energy values in effective Hartree energy ($E_h^*$) scale of each geometry.

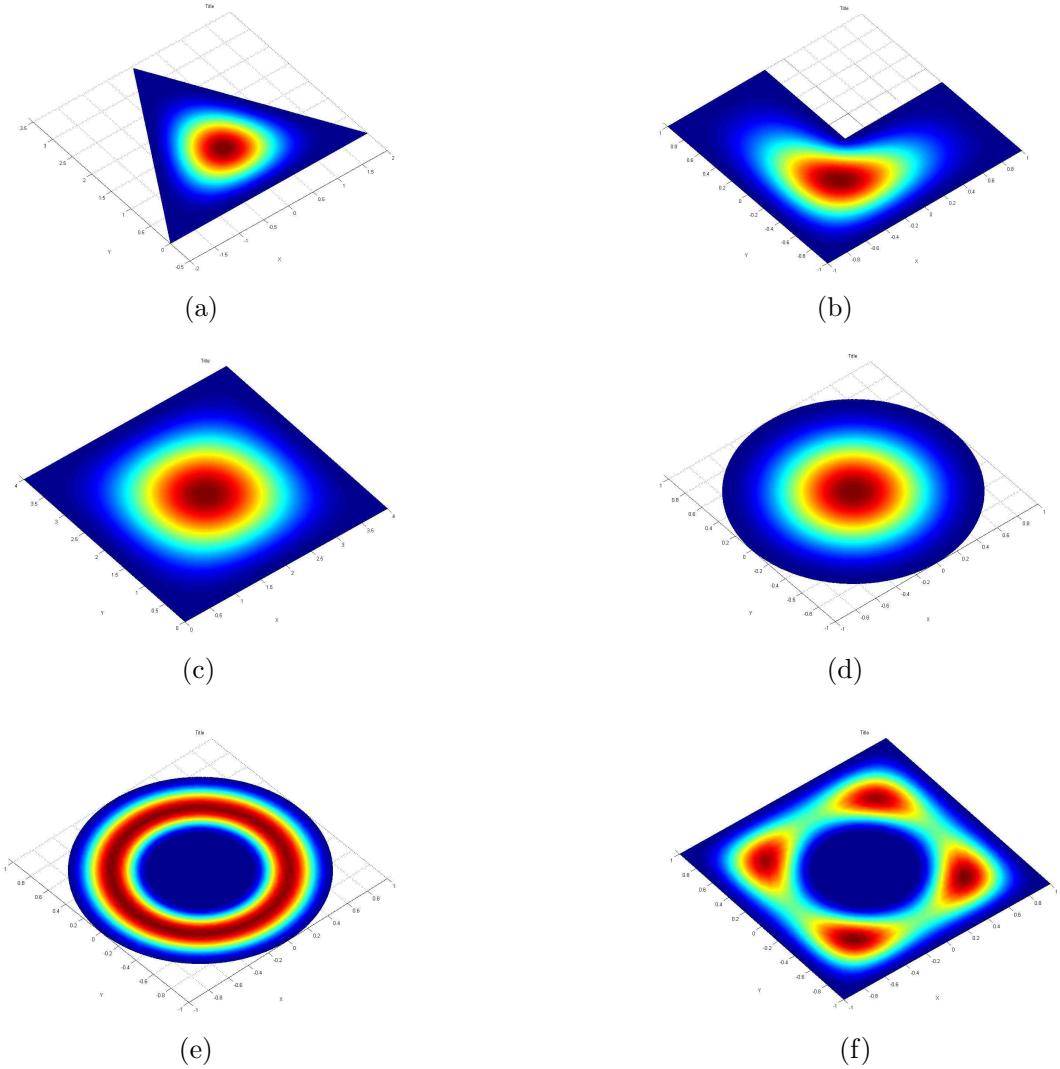

(a) (b) (c) (d) (e) (f)

Figure 4.23 Ground state localizations of single particle in a quantum wire like (a)triangular, 0.3338 $E_h^*$ (b) L shape 0.9831 $E_h^*$ (c) square 0.1252 $E_h^*$, (d) circle 0.5868 $E_h^*$ (e) circle with hole 2.7422 $E_h^*$, (f) square with hole 2.0044 $E_h^*$

### *4.2.5 More about The Exciton Problem*

In this section, the charge localizations of the exciton problem for different angular momentum quantum numbers for center of mass and relative parts are given in Figure 4.24 and Figure 4.25, respectively. Table 4.5 presents the energy values of the Center of mass part of the problem. This part of the problem has Harmonic oscillator like Hamiltonian. This Hamiltonian has a analytical solution which is;

$$\varepsilon_{n,l} = \hbar\omega(2n + l + \frac{d}{2}) \tag{4.2.17}$$

Table 4.5 Harmonic oscillator energy values, namely the center of mass part energies for appropriate coefficients. 9 energy levels for different angular momentum quantum number (also a parameter in the numerical FEM code) are given. Energies are $\hbar\omega$ units.

| $n$ | $l = 0$ | $l = 1$ | $l = 2$ |
|---|---|---|---|
| 0 | 1.5000000000 | 2.5000000000 | 3.5000000000 |
| 1 | 3.5000000000 | 4.5000000000 | 5.5000000000 |
| 2 | 5.5000000000 | 6.5000000000 | 7.5000000000 |
| 3 | 7.5000000000 | 8.5000000000 | 9.5000000000 |
| 4 | 9.5000000000 | 10.5000000000 | 11.5000000000 |
| 5 | 11.5000000000 | 12.5000000000 | 13.5000000000 |
| 6 | 13.5000000000 | 14.5000000000 | 15.5000000000 |
| 7 | 15.5000000000 | 16.5000000000 | 17.5000000000 |
| 8 | 17.5000000000 | 18.5000000000 | 19.5000000000 |

Here $n$ is principal quantum number, $l$ is angular momentum quantum number and $d$ represents the dimension of the problem. table 4.6 presents the similar data of the relative part of the exciton problem in $\hbar\omega$ energy scale. The ground state energy graphics depending on the quantum dot sizes for relative and center of mass parts are also showed in Figure 4.26. Three more excited state localizations are presented additional to the ground state. In localization calculations, quantum dot size is taken ten effective Bohr raious ($10a^*$). The other parameters used in the calculations are like that: Number of global elements : 42, Number of nodes : 8 (namely, used 8th order basis functions). One can see the results in the figures

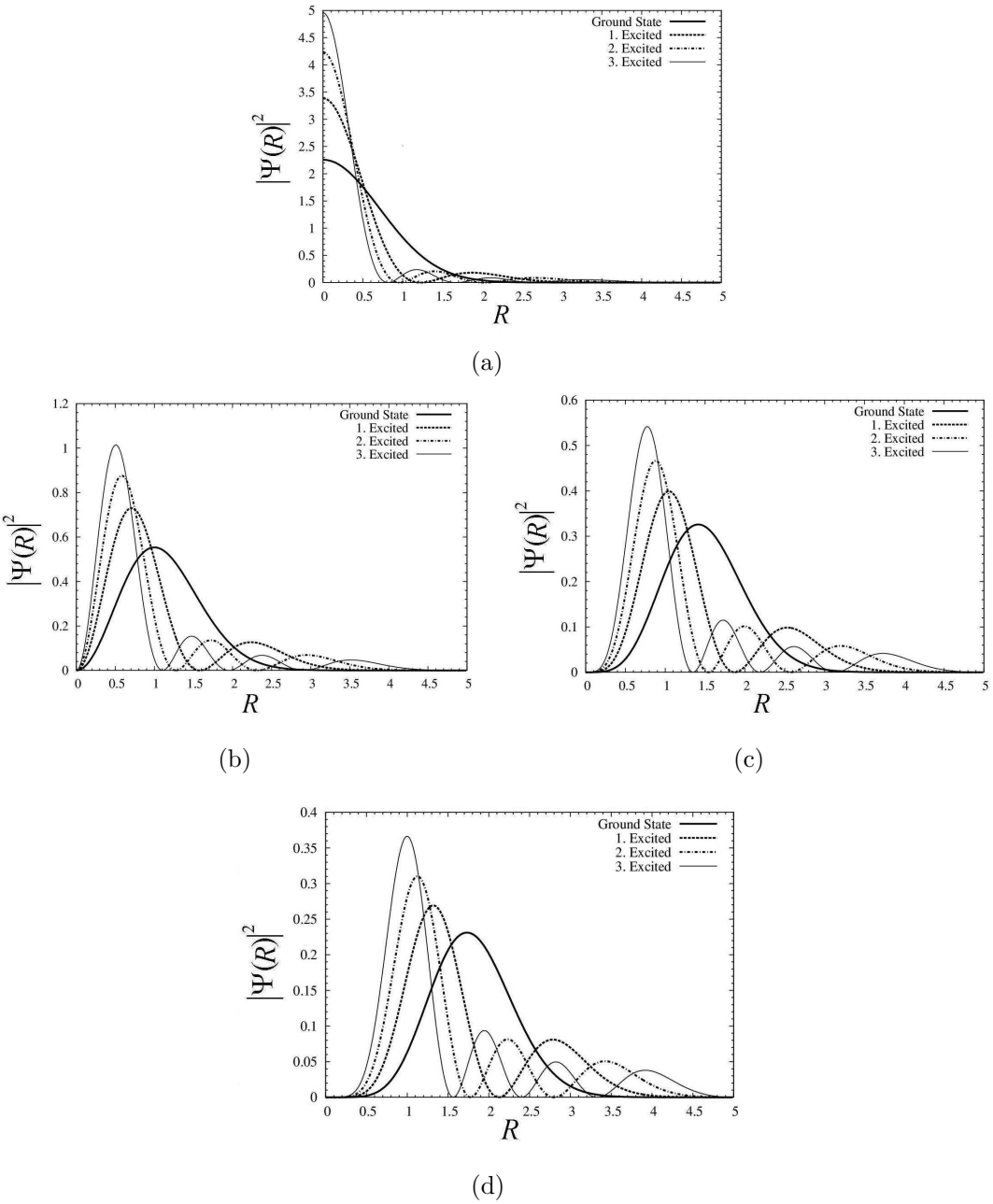


Figure 4.24 Ground state and first three excited state localizations of the center of mass part in the exciton problem for (a) $l = 0$ (b) $l = 1$ (c) $l = 2$ (d) $l = 3$. Here, plots are showed in the interval $0 < R < 5a^*$ for good viewing.

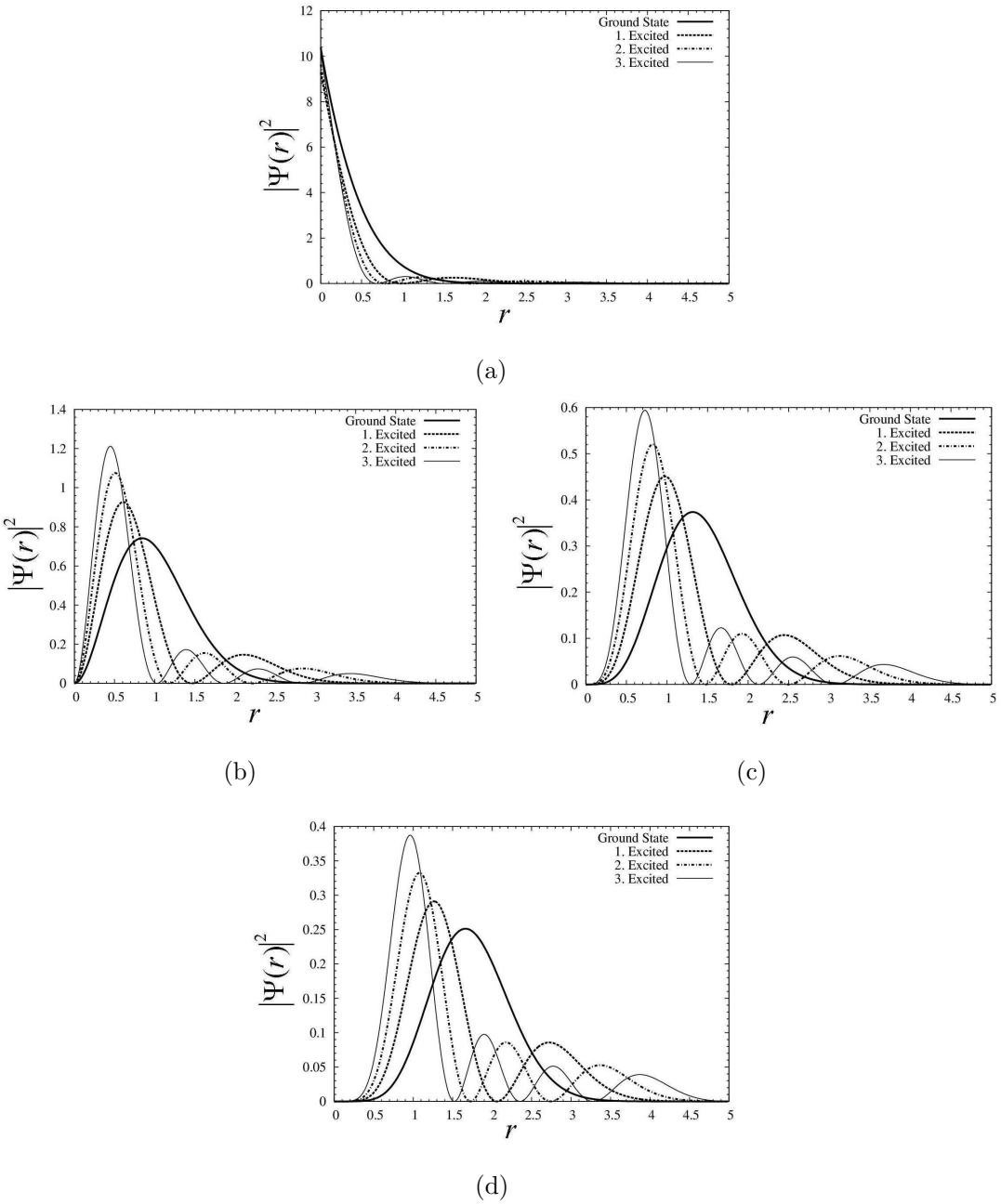


Figure 4.25 Ground state and first three excited state localizations of the relative part in the exciton problem for (a) $l = 0$ (b) $l = 1$ (c) $l = 2$ (d) $l = 3$. Here, plots are showed in the interval $0 < r < 5a^*$ for good viewing.

Table 4.6 Exciton energy values, namely the relative part energies for appropriate coefficients. 9 energy levels for different angular momentum quantum number (also a parameter in the numerical FEM code) are given. Energies are $\hbar\omega$ units.

| $n$ | $l=0$ | $l=1$ | $l=2$ |
|---|---|---|---|
| 0 | 0.8926027396 | 2.1145895312 | 3.1951989292 |
| 1 | 3.0145292803 | 4.1562994241 | 5.2179969025 |
| 2 | 5.0733048564 | 6.1836003485 | 7.2348272418 |
| 3 | 7.1108547881 | 8.2035871843 | 9.2480463176 |
| 4 | 9.1379189893 | 10.2191885043 | 11.2588582060 |
| 5 | 11.1588046190 | 12.2318863680 | 13.2679581151 |
| 6 | 13.1756516036 | 14.2425304168 | 15.2757824012 |
| 7 | 15.1896703175 | 16.2516509482 | 17.2826221620 |
| 8 | 19.2119574778 | 20.2666229745 | 21.2941059784 |

and tables. The results have very high accuracy because of the method (FEM) that used in the numerical calculations.

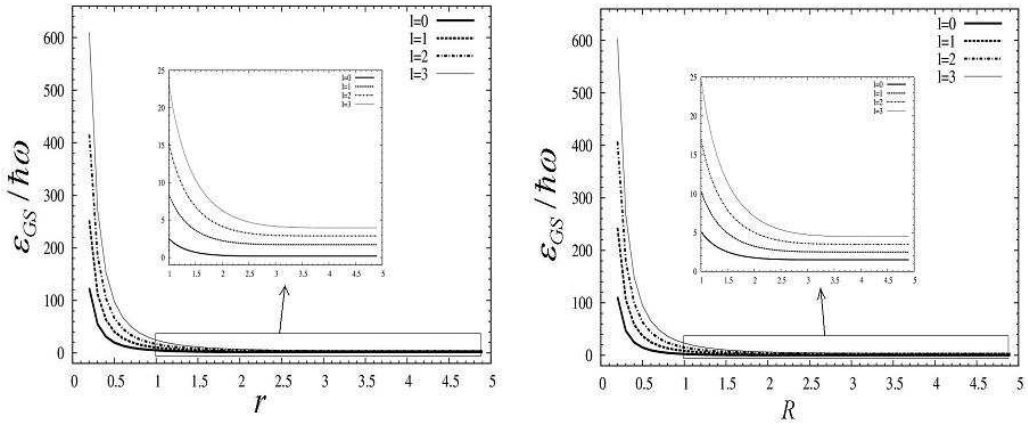


Figure 4.26 Ground state energies versus quantum dot size for $l=0,1,2,3$ in $\hbar\omega$ scale. The plot on the left and right sides belong to relative part and center of mass part, respectively.

# CHAPTER FIVE
# CONCLUSION

The main objectives of this work have been calculating the electronic structure of the quantum wires. From this point of view, emphasis has also been set on developing and testing the computational method called Finite Element Method which is useful and powerful in these calculations. The method and the program codes have been controlled and tested with simple known problems which have analytical solutions for the validity of the method.

In this work we proposed an efficient numerical method for calculating the electronic structure of low dimensional systems such as quantum dots and quantum wires including not only the ground state energy but also higher energy levels by using area coordinates and Finite Element Method. In this respect, single charged particle problem under parabolic and linear confinement in six different quantum wire cross-sections are investigated. Also, an exciton system in a parabolic GaAs quantum dot problem is studied with a high accuracy additional to single particle problem in QW. This problem has a high spherical symmetry. This allowed us to reduce the dimensionality of the problem from 3D to 1D. All calculations are done with the numerical method called Finite element method. FEM is a very important tool of scientific and engineering analysis. Using area coordinates with FEM, especially in QW calculations, provides us a significant simplification to form the matrix elements and also to calculate the integrals in two dimensions.

In this thesis it has been introduced an computationally efficient approach for the matrix elements and area coordinates which are used to simplify calculating global element areas and integrals in these global elements which in an unstructured mesh for the single particle problem. The boundaries of the integrals make the integral calculations harder in the cartesian coordinates, especially in

two dimensions with triangle elements. Using area coordinates with FEM provides us a significant simplification to form the matrix elements and also to calculate the integrals in two dimensions.

As a second problem, exciton states in a parabolic quantum is investigated. Here, the problem have been considered in two energy scales (effective Hartree energy and $\hbar\omega$) and the energy spectrums versus confinement and interaction parameters have also been presented with very high accuracy. In this problem, an electron and a light hole form the excitonic system in GaAs semiconductor quantum dot with parabolic confinement. In the other word, the quantum dot system that we discussed consist of an electron and a light hole in GaAs semiconductor.

Increasing the quality of MG with FEM for Quantum Rods and Quantum Tetrapod systems could be counted for the future works of this thesis. Therefore, the electronic structures, charge localizations, electronic transitions in QW lattices, tunneling and optical properties could be respected among the future works.

## REFERENCES

Arakawa, Y., & Sakaki, H. (1982). Multidimensional quantum well laser and temperature dependence of its threshold current. *Appl. Phys. Lett. 40*, 939.

Arakawa, Y., & Yariv, A. (1986). Quantum well lasers–Gain, spectra, dynamics. *IEEE J. Quantum Electron. QE-22*, 1887-1889.

Banyai, L., Koch, J. S. (1993). *Semiconductor Quantum Dots*. Singapore: World-Scientific.

Bern, M., & Plassmann, P. (1999). *Handbook of Computational Geometry: Mesh generation*. Amsterdam: Elsevier Science.

Bloomenthal, J. (1998). Polygonization of implicit surfaces. *Comput. Aided Geom. Design, 5(4)*, 341-355.

Bossen, F. J., & Heckbert, P. S. (1996). *A pliant method for anisotropic mesh generation. In Proceedings of the 5th International Meshing Roundtable*. Sandia Nat. Lab.

Bruss, L. E. (1986). Electron-electron and electron-hole interactions in small semiconductor crystallites: The size dependence of the lowest excited electronic state. *J. Chem. Phys., 80*, 4403.

Bruss, L. E. (1986). Exact quantization of the scattering from a classically chaotic repellor. *J. Chem. Phys., 90*, 2255.

Citrin, D. S., & Chang, Y. C. (1989). Valence-subband structures of $GaAs/Al_xGa_{1-x}As$ quantum wires: The effect of split-off bands. *Phys. Rev. B, 40*, 5507.

Dempsey, J., Johnson, N. F., Brey, L., & Halperin, B. I. (1990). Collective modes in quantum-dot arrays in magnetic fields. *Phys. Rev. B, 42*, 11708.

Desbrun, M., Tsingos, N., & Gascuel, M-P. (1996). Adaptive sampling of implicit surfaces for interactive modelling and animation. *Computer Graphics Forum, 15(5)*, 319-325.

Edelsbrunner, H. (2001). *Geometry and topology for mesh generation, volume 7 of Cambridge Monographs on Applied and Computational Mathematics.* Cambridge: Cambridge University Press.

Figueiredo, L. H. de F., Gomes, J. de M., Terzopoulos, D. & Velho, L. (1992). *Physically-based methods for polygonization of implicit surfaces: In Proceedings of the conference on Graphics interface 92.* Morgan Kaufmann Publishers Inc.

Gangopadhyay, S. & Nag, B. R. (1997). Energy levels in finite barrier triangular and arrowhead-shaped quantum wires. *J.Appl.Phys., 81*, 7885.

Garm, T. (1996). Exciton states in spherical parabolic GaAs quantum dots. *J. Phys.: Condens. Matter, 8*, 5725.

Giorgi, M. De., Tari, D., Manna, L., Krahne, R., & Cingolani, R. (2005). Optical properties of colloidal nanocrystal spheres and tetrapods. *Microelectronics Journal, 36*, 552-554.

Gloth, O., & Vilsmeier, R. (2000). *Level Sets as Input for Hybrid Mesh Generation. In Proceedings of the 9th International Meshing Roundtable.* Sandia Nat. Lab.

Harrison, P. (2002). *Quantum Wells, Wires and Dots: Theoretical and Computational Physics.* New York: Wiley.

Hu, J., Wang, L. W., Li, L. S., Yang, W., & Alivisatos, A. P. (2002). Semiempirical Pseudopotential Calculation of Electronic States of CdSe Quantum Rods. *J. Phys. Chem. B, 106*, 2447-2452.

Hu, Y. Z., Lindberg, M., & Koch, S. W. (1990). Theory of optically excited intrinsic semiconductor quantum dots. *Phys. Rev. B, 42*, 1713-1723.

Hui, P. (2004). Quantum-confinement effects on binding energies and optical properties of excitons in quantum dots. *Chin. Phys. Lett., 21*, 160-163.

Hutton, D. V., (2004). *Fundamental of Finite Element Analysis*. New York: McGraw-Hill.

Ikezawa, M., Nair, S. V., Ren, H., Masumoto, Y. & Ruda, H. (2006). Biexciton binding energy in parabolic GaAs quantum dots. *Phys. Rev. B, 73*, 125321.

Ishigaki, T., Ogawa, M., Morita, M., & Miyoshi, T. (2002). Analysis of subband structures and optical properties of periodic strained quantum wires by a finite element method. *J. Appl. Phys., 91*, 5815-5819.

Jaziri, S., & Bennaceur, R. (1995). Excitonic properties in GaAs parabolic quantum dots. *J.Phys.III France, 5*, 1565-1572.

Johnson, N. F., & Payne, M. C. (1991). Exactly solvable model of interacting particles in a quantum dot. *Phys Rev Lett, 67*, 1157-1160.

Kayanuma, Y. (1991). Wannier excitons in low-dimensional microstructures: shape dependence of the quantum size effect. *Phys. Rev. B, 44*, 13085-13088.

Kelly, M. J. (1995). *Low dimensional semiconductors: Materials, physics, technology, devices*. Oxford: Clarendon Press.

Kojima, K., Mitsunaga, K., & Kyuma, K. (1989). Calculation of two-dimensional quantum-confined structures using the finite element method. *Appl. Phys. Lett., 55*, 882.

Kwon, Y. W., & Bang, H. (2000). *The Finite Element Method using MATLAB*. New York: CRC Press.

Lee, K. Y., Smith, T. P., Arnot, H., Knoedler, C. M., Kern, J. M., & Laux, E. (1988). Fabrication and characterization of one- and zero-dimensional electron systems. *J. Vac. Sci. Technol. B, 6*, 1856-1860.

Li, Z., Zhang, Y., Wang, H., & Xiao, J. (2006). Internal Excited State of the Strong Coupling Exciton in Polar Crystals Quantum Dot. *Chinese Journal of Luminesence, 27/5* 641-645.

Loss, D. & DiVincenzo, D. P. (1998). Quantum computation with quantum dots. *Phys. Rev. A, 57*, 120.

Moler, C. (2004). *Numerical Computing with MATLAB*. Siam.

Molino, N., Bridson, R., Teran, J. & Fedkiw, R. (2003). *A Crystalline, Red Green Strategy for Meshing Highly Deformable Objects with Tetrahedra. In Proceedings of the 12th International Meshing Roundtable*. Sandia Nat. Lab.

Nakamura, K. Shimizu, A., Koshiba, M., Hayata, K. (1989). Finite-element analysis of quantum wells of arbitrary semiconductors with arbitrary potential profiles. *IEEE J. of Quantum Electronics, 25*, 889-895.

Ogawa, M., Kunimasa, T., Ito, T., & Miyoshi, T. (1998). Finite-element analysis of quantum wires with arbitrary cross sections. *J. Appl. Phys., 84*, 3242.

Owen, S. J. (1998). *A survey of unstructured mesh generation technology. In Proceedings of the 7th International Meshing Roundtable*. Sandia Nat. Lab.

Park, S-H., Ahn, D., & Lee, Y-T. (2004). Finite element analysis of valence band structures in quantum wires. *J. App. Phy., 96.*, (4) 2055–2062.

Pask, J. E., Klein, B. M., Sterne, P. A., & Fong, C. Y. (2001). Finite-element methods in electronic-structure theory. *Comp. Phys. Comm., 135*, 1-34.

Persson, P. (2005). *Mesh Generation for Implicit Geometries*. Massuchusets: Ph.D. Thesis

Proetto C. R. (1992). Self-consistent electronic structure of a cylindrical quantum wire. *Phys. Rev. B, 45*, 11911.

Pryor, C. (1991). Electronic structure and optical properties of serpentine superlattice quantum-wire arrays. *Phys. Rev. B, 44*, 12912.

Ram-Mohan, L. R. (2002). *Finite Element and Boundary Element Applications in Quantum Mechanics*. New York: Oxford Uni. Press.

Ruppert, J. (1995). A Delaunay refinement algorithm for quality 2-dimensional mesh generation. *J. Algorithms, 18(3)*, 548-585.

Said, M. E. (1994). The ground-state energy of an exciton in a parabolic quantum dot. *Semiconductor Sci. Tech., 9*, 272.

Sakiroğlu, S., Doğan, Ü., Yıldız, A., Akgüngör, K., Epik, H., Ergün, Y., Sarı, H. & Sökmen, İ. (2009). Ground state energy of excitons in quantum dot treated variationally via Hylleraas-like wavefunction. *Chin. Phys. B, 18*, 1578-1585.

Searles, D. J., & von Nagy-Felsobuki, E. I. (1988). Numerical experiments in quantum physics: Finite-element method. *Am. J. Phys., 56*, 444-448.

Shewchuk, J. R. (2002). Delaunay refinement algorithms for triangular mesh generation. *Comput. Geom., 22(1-3)*, 21-74.

Shimada, K., & Gossard, D. C. (1995). *Bubble mesh: automated triangular meshing of non-manifold geometry by sphere packing. In SMA 95: Proceedings of the Third Symposium on Solid Modeling and Applications.*

Sikorski, C., & Merkt, U. (1989). Specroscopy of electronic states in InSb quantum dots. *Phys. Rev. Lett., 62*, 2164-2167.

Sweeny, M., Xu, J., & Shur, M. (1988). Hole subbands in one-dimensional quantum well wires. *Superlattices Microstruct., 4*, 623-626.

Szeliski, R. & Tonnesen, D. (1992). *Surface modeling with oriented particle systems. In SIGGRAPH 92: Proceedings of the 19th annual conference on Computer graphics and interactive techniques.* ACM Press.

Thao, T. H., & Viet, N. A. (2004). Binding energy of exciton in quantum dots with the central-cell correction depending on the dot size. *Communications in Physics, 14*, 95-99.

Tkach, M. V., Seti, J. O. (2007). Exciton in closed and opened quantum dot. Cond. Matt. Phys. *Condensed Matter Physics, 10*, 23-31.

Witkin, A. P., & Heckbert, P. S. (1994). *Using particles to sample and control implicit surfaces. In SIGGRAPH 94: Proceedings of the 21st annual conference on Computer graphics and interactive techniques.* ACM Press.

Wixforth, A., Kaloudis, M., Rocke, C., Ensslin, K., Sundaram, M., English, J. H., & Gossard, A. C. (1994). Dynamic response of parabolically confined electron systems. *Semicond. Sci. Tech., 9*, 215-240.

Woggon, U. (1997). *Optical Properties of Semiconductor Quantum Dots.* Springer Verlag.

Xie, W. F. (2006). Binding energies of an exciton in a Gaussian potential quantum dot. *Chin. Phys., 15*, 203.

Yamauchi, T., Takahasi, Y. T., & Arakawa, Y. (1991). Tight binding analysis for quantum-wire lasers and quantum-wire infrared detectors. *IEEE J. Quantum Electron., 27*, 1817-1823.

Yariv, A. (1988). Scaling laws and minimum threshold currents for quantum-confined semiconductor lasers. *Appl. Phys. Lett., 53*, 1033.

Yi, J. C., & Dagli, N. (1995). Finite-element analysis of valence band structure and optical properties of quantum-wire arrays on vicinal substrates. *IEEE J. Quantum Electron., 31*, 208.

Yildiz, A., Şakiroğlu, S., Doğan, Ü., Akgüngör, K., Epik, H., Ergün, Y., Sarı, H. & Sökmen, İ. (2009). Variational computations for excitons in quantum dots:

A Quantum Monte Carlo Study. *International Journal of Modern Physics B*, (Accepted to publish on March 31,2009).